Journal of Environmental Management 410 (2026) 130107

Contents lists available at ScienceDirect

Journal of Environmental Management

journal homepage: www.elsevier.com/locate/jenvman

Research article

Sewage sludge biochar-based fertilizer enriched with K-bearing silicate agrominerals and oxalic acid: physicochemical characterization and carbon stability

Marcela Granato Barbosa dos Santos [a], José Ferreira Lustosa Filho [a], Camila Rodrigues Costa [a], Beatriz Carvalho Lima [a], Maíra Lopes D'Ávila [a], Sérgio Sirilo de Oliveira [a], Gilberto de Oliveira Mendes [b], Éder de Souza Martins [c], Giuliano Marchi [c], Cícero Célio de Figueiredo [a,*]

[a] Faculty of Agronomy and Veterinary Medicine, University of Brasília, Brasília, Federal District, 70910-970, Brazil
[b] Institute of Agricultural Sciences, Federal University of Uberlândia, Monte Carmelo, Minas Gerais, 38500-000, Brazil
[c] Brazilian Agricultural Research Corporation, Embrapa Cerrados, Planaltina, Federal District, 73310-970, Brazil

ARTICLE INFO

Keywords:
Organic acids
Carbon stability
Multinutrient fertilizers
Pyrolysis
Remineralizers

ABSTRACT

The synthesis of biochar-based fertilizers (BBFs) from urban waste and agrominerals represents a promising approach to advancing a circular economy and agricultural sustainability. In this study, 16 BBFs were synthesized from pyrolyzed sewage sludge biochar at 300 °C and 500 °C (SSB300 and SSB500), potassium-rich silicate agrominerals (ASi) such as mica schist and phonolite, and different concentrations of oxalic acid (OA): 0; 0.33; 0.67 and 1 mol L^{-1}. The formulations were characterized in terms of chemical, physical, and mineralogical composition, structural properties, and carbon (C) stability. The pyrolysis temperature was the main factor responsible for the structural stability of C. Materials produced at 500 °C showed greater aromaticity, lower H/C and O/C ratios, lower ratios between volatile material (VM) and fixed C (FC) (VM/FC), and higher recalcitrance (R_{50}) and thermostable fraction (TSF) values, indicating greater recalcitrance and structural stability, with emphasis on SSB500+Mica + OA_0 and SSB500+Phon + OA_0. In contrast, formulations with SSB at 300 °C exhibited greater surface functionalization and enhanced potential for chemical reactivity, particularly at higher OA concentrations, with emphasis on SSB300+Phon + OA_1. The OA application altered the mineral matrix and the structure of C, promoting greater surface functionalization and potentially nutrient availability, although with a slight reduction in C recalcitrance. The incorporation of ASi increased the total K content and promoted mineral compositional differentiation in the new fertilizers. The results suggest that the developed BBFs constitute highly tunable organomineral systems, in which the manipulation of pyrolysis temperature and chemical activation enables targeted modulation of the balance between C structural stability and reactivity. Although OA reduces the stability of C, our results show that it is possible to synthesize formulations tailored either for greater structural stability (SSB500-based) or for enhanced reactivity and potential nutrient release (SSB300+OA-based), depending on the intended agronomic application. This approach may contribute to the rational design of multifunctional fertilizers, enabling the development of formulations tailored to diverse management strategies and soil conditions.

1. Introduction

Wastewater treatment processes generate two main products: treated water and sewage sludge (SS). Treated water is discharged into receiving water bodies, while SS must be treated and properly disposed (Kanteraki et al., 2022). Sewage sludge management represents a global challenge, with annual production of approximately 100 million dry tons, equivalent to approximately 35–85 g of dry matter per capita per day, and projected to reach 175 million tons by 2050 (Patel et al., 2026; Werle and Sobek, 2019; Wijesekara et al., 2016). Its agricultural use has

* Corresponding author.
E-mail address: cicerocf@unb.br (C.C. Figueiredo).

https://doi.org/10.1016/j.jenvman.2026.130107
Received 7 April 2026; Received in revised form 16 May 2026; Accepted 29 May 2026
Available online 2 June 2026

been considered a promising alternative with the potential to increase soil organic matter and nutrient content such as phosphorus (P), nitrogen (N), calcium (Ca), and zinc (Zn) (Li et al., 2024; Zhang et al., 2017). However, the use of raw SS can carry contaminants (Zhang et al., 2017) such as pathogenic microorganisms (H. Zhang et al., 2022), organic pollutants (Košnář et al., 2023), and heavy metals (Tariq, 2021), which are harmful to humans and the ecological system (Hoang et al., 2022). Therefore, if not treated properly, SS can cause serious pollution to the environment.

A promising alternative for SS treatment is pyrolysis, a thermochemical process that exposes organic materials to high temperatures under oxygen-limited conditions (Lehmann and Joseph, 2024; Rydgård et al., 2024; Sivaranjanee et al., 2023). This process produces three main products: biochar, biogas, and bio-oil. Among these pyrolysis co-products, biochar has significant agronomic importance because it concentrates the mineral content of the original material (SS), containing high levels of C, humic and fulvic acids, nutrients such as P, N, Ca, and Zn, as well as ash (Kacprzak et al., 2025; Paz-Ferreiro et al., 2018). In addition, biochar typically has an alkaline pH, an abundance of surface functional groups, and inorganic compounds such as carbonates and metallic oxides—characteristics that support pH correction, nutrient retention, and contaminant immobilization in soil (Fachini et al., 2021; Panahi et al., 2020; Paz-Ferreiro et al., 2018; Volpi et al., 2024).

Compared to other organic wastes, SS has high concentrations of nitrogen (N) (Cui et al., 2025) and total P (Cui et al., 2025; Lustosa Filho et al., 2025). This occurs because during wastewater treatment, salts such as aluminum sulfate or chloride are added, which flocculate particles dispersed in water containing N and P, leaving them concentrated in the final SS mass (Cui et al., 2025). On the other hand, potassium (K), because it does not integrate structural organic compounds and is highly soluble, remains predominantly in the liquid phase during wastewater treatment. This process results in a sewage sludge biochar (SSB) with typically low levels of this element (0.2–1.7%) (Xu et al., 2017). Therefore, to transform SSB into a nutrient-balanced fertilizer, the addition of K sources is necessary. These sources can be either conventional potassium fertilizer, i.e., KCl (Fachini et al., 2021, 2022, 2024; Ndoung et al., 2023), or alternative sources (Santos et al., 2026). A promising alternative source is silicate agrominerals (ASi), including soil remineralizers (REM) and silicate fertilizers (FSi) (Martins et al., 2026; Santos et al., 2026). These materials originate from nutrient-rich rocks, including K-rich silicate minerals such as feldspars and micas, which can contain more than 10% K_2O (Van Straaten, 2007). However, K feldspars are formed by tetrahedral groups of silicon (Si) and aluminum (Al), strongly linked together by cations, with K inserted into the crystalline structure, making its extraction difficult and rendering K unavailable to plants in the short term (Melo and Alleoni, 2019; Santos et al., 2026; Skorina and Allanore, 2015; Van Straaten, 2007). Despite the presence of trioctahedral micas, in which K from the interlayer more readily enters solution (Krahl et al., 2022b), integrating rocks rich in these minerals with a solubilizing agent, such as low-molecular-weight organic acids, increases the potential to release this nutrient.

Organic acids are efficient mineral solubilizers (Duarte et al., 2022; Lodi et al., 2022; Santoyo et al., 2026). Naturally present in the soil, these acids originate from plant root exudates, the decomposition of organic matter, and microbial metabolites (Liu et al., 2017; Zhang et al., 2020). Oxalic acid (OA) has stood out among organic acids with high potential for solubilizing nutrients (Lodi et al., 2022; Mendes et al., 2020; Santos et al., 2024, 2026), in addition to showing great potential and improving the performance of biochar-based fertilizers (BBFs) (Lustosa Filho et al., 2026). Thus, enriching SSB with ASi in the presence of organic acids, such as OA, could generate sustainable fertilizers applicable at reduced rates compared to pure biochar.

In addition to the nutritional dimension, enriched BBFs are also relevant in the context of climate change. Biochar is characterized by containing aromatic and structurally stable C chains (Adhikari et al., 2024; Costa et al., 2025; Halalsheh et al., 2024), contributing to C sequestration in the soil, along with mitigation of greenhouse gases and increased crop productivity (Button et al., 2022; Jones et al., 2026; Zhou et al., 2023). In parallel, silicate minerals can capture atmospheric C dioxide (CO_2) through accelerated weathering (Enhanced Rock Weathering – ERW), culminating in the formation of carbonates and bicarbonates (Fei et al., 2025; Xu et al., 2024). The agricultural sector accounts for approximately 18.3% of global greenhouse gas emissions, with about 4% attributable to fertilizer use (Boehm et al., 2023). In this context, the development of fertilizers with multifunctional characteristics that combine nutritional supply, potentially slow nutrient release to reduce losses through leaching and volatilization (Gebretsadkan et al., 2024; Raj et al., 2021), and mitigation of greenhouse gas emissions constitutes a relevant strategy for sustainable agriculture. Thus, the integration of these technologies can represent a strategic advance in the transition to low-C agricultural systems.

Although the agronomic potential of SSB and ASi is well known, uncertainties remain regarding the integrated performance of fertilizers produced by combining SSB, K-rich silicate minerals, and OA. There are uncertainties regarding the impact of mineral enrichment and the action of organic acids on the structural stability of C of these materials, as well as on the simultaneous interaction of their nutritional properties. Previous studies have generally evaluated these components separately or in simplified combinations (Duarte et al., 2022; Mendes et al., 2022; Santos et al., 2024, 2026), and there is still a lack of an integrated understanding of how pyrolysis temperature, mineral composition, and organic acid activation simultaneously influence nutrient availability and C structural stability. Although organic acids may increase nutrient solubilization, they may also reduce C stability. This trade-off remains poorly understood in biochar-based organomineral fertilizers.

Therefore, our hypothesis is that enriching SSB with K-rich ASi, in the presence of OA, promotes the solubilization of structurally unavailable nutrients and generates multifunctional fertilizers in which increased total K content, potential nutrient reactivity and high C stability are modulated by production conditions, resulting in materials with agronomic potential and potential for greater C persistence in soil. In view of this, the present study aimed to characterize BBFs produced from SS enriched with ASi and OA, evaluating their chemical composition, thermal stability, and indicators associated with C stability and persistence potential.

2. Material and methods

2.1. Acquisition and preparation of feedstocks

The SSB was produced from SS collected at the Melchior Wastewater Treatment Plant, operated by the Environmental Sanitation Company of the Federal District, Brasília, DF, Brazil. The SS was initially air-dried to approximately 10% moisture, crushed, and sieved through a 4 mm mesh. Then, the SS was subjected to pyrolysis in a muffle furnace (Linn Elektro, Eschenfelden, Germany) at temperatures of 300 °C and 500 °C (SSB300 and SSB500), with an average heating rate of 2.5 °C min^{-1} and a residence time of 5 h. After pyrolysis, the carbonized material was again crushed and sieved through a 1 mm mesh. These temperatures were selected because they represent contrasting pyrolysis conditions widely used in the literature, thereby enabling the production of materials with varying degrees of carbonization. While lower temperatures (~300 °C) tend to preserve more functional groups and higher chemical reactivity, higher temperatures (~500 °C) promote greater aromaticity and structural stability of C, enabling evaluation of how these characteristics affect the balance between nutrient availability and C stability.

The ASi used in the study were two ground potassium-rich silicate rocks: phonolite and mica schist, abbreviated as Phon and Mica, respectively. According to the ASi classification of Martins et al. (2026), phonolite is a K-Asi (CaO + MgO + K_2O > 9% and <20%, >8% K_2O), and mica schist is a KMgCa-Asi (CaO + MgO + K_2O > 9% and <20%,

between 3 and 8% K_2O). The choice of agrominerals was based on their mineralogical differences and contrasting K release behavior, with Phon rich in minerals that are more resistant to dissolution and Mica composed of more reactive phases. Since K availability is primarily controlled by mineralogy and dissolution kinetics rather than by total content alone, these materials enable evaluation of distinct responses to chemical activation. Phon was collected in the municipality of Poços de Caldas, Minas Gerais, Brazil, while Mica originated from waste from the production of crushed stone for civil construction in the municipality of Abadiânia, Goiás, Brazil. Both materials were crushed and classified by particle size using a 1 mm sieve before use. The chemical and physical characteristics of the biochar and agrominerals are presented in Table 1, and detailed information about the materials, obtained by different analytical techniques, is presented in Fig. S1. The OA solutions were prepared at concentrations of 0.33 mol L^{-1}, 0.67 mol L^{-1} and 1 mol L^{-1}, using OA from Sigma-Aldrich® (Merck, Darmstadt, Germany). The OA concentrations were defined based on previous studies demonstrating their efficiency in solubilizing nutrients in biochar and silicate minerals (Santos et al., 2024, 2026) allowing the evaluation of different levels of chemical activation.

2.2. Production of fertilizers

The fertilizers were obtained from the physical mixing of SSB with ASi followed by the addition of the corresponding acid solution. The proportions were chosen to achieve a balance between the nutrients N, P, and K, obtaining K with the addition of ASi and P and N with the addition of SSB. The production method and material proportions are specified in Fig. 1 and Table 2. The aim was to achieve a K concentration as close as possible to 2%, based on the total K concentration determined by extracting ASi with hydrofluoric and perchloric acids, while ensuring no significant loss of P and N from the SSBs, keeping them between 1% and 2%. Thus, approximately 21% Phon and 50% Mica were added to the mixture.

The resulting mixture was dried in an oven at 40 °C for 48 h. After this initial drying, the material was ground, sieved through a 1 mm mesh, and then 65 g kg^{-1} of pre-gelatinized starch was added, used as a binding agent for the formation of the granules. Finally, the BBFs were then subjected to drying in an oven at 40 °C for 24 h (Fig. 1).

The combination of pyrolysis temperature, agromineral type, and OA concentration resulted in 16 distinct BBF formulations (Table 2).

2.3. Physicochemical and mineralogical characterization of BBFs

The formulated fertilizers underwent chemical characterization. pH, macro- and micronutrient, and heavy metal analyses were performed according to the Official Analytical Methods Handbook for Fertilizers and Soil Amendments (Brasil, 2017). pH was determined in 0.01 M $CaCl_2$ (1:5, w/v) using a PHS-3B meter (Guangdong, China). Macronutrients were quantified after nitroperchloric extraction: P by spectrophotometry (400 nm) (SP 22 Automatic Digital Spectrophotometer, China), K by flame photometry, and Ca, Mg, and S by ICP-OES (ICPE-9000, Shimadzu). Micronutrients and heavy metals were determined according to USEPA SW-846 3050B (Environmental Protection Agency, 1996), with measurements performed using ICP-OES (ICPE-9000, Shimadzu, Japan).

The samples were also subjected to elemental analysis (C, N, and H). After grinding, maceration, and sieving (0.150 mm), approximately 1 mg of each sample was weighed into tin capsules and analyzed by dry combustion in a CHN analyzer (Euro EA3000 Elemental Analyzer, Milan, Italy). The oxygen (O) content was calculated by the difference between the percentage of ash and the elemental contents of C, H, N, and S.

The percentages of moisture, VM, ash, and FC were determined according to ASTM (American Society for Testing and Materials, 2013). Moisture was obtained by measuring the mass loss after drying the samples in an oven at 105 °C until constant mass was reached. VM was quantified by measuring the mass loss resulting from heating the samples at 950 °C for 7 min in a muffle furnace (Linn-Elektro Therm, model KK 260 SO 4060). Ash content was determined by calcining the samples at 750 °C for 6 h. Fixed carbon was calculated by difference, considering the dry mass of the samples.

Energy-dispersive X-ray fluorescence spectroscopy (EDX) was performed on an EDX-720HS (Shimadzu). Powder X-ray diffraction (XRD) was conducted using a D8 Focus diffractometer (Bruker), with Cu Kα radiation (40 kV, 30 mA), 2θ scan between 10° and 70°, 0.05° increment

Table 1
Chemical and physical characteristics of sewage sludge biochars (SSB300 and SSB500) and silicate agrominerals (mica schist and phonolite).

Parameters	SSB300	SSB500	Mica schist	Phonolite
pH	6.10 ± 0.08 b	6.23 ± 0.12 ab	6.33 ± 0.05 ab	6.37 ± 0.05 a
P_{Total} (%)	2.77 ± 0.18 a	3.28 ± 0.49 a	0.17 ± 0.03 b	0.11 ± 0.04 b
Ca (%)	0.57 ± 0.05 b	0.86 ± 0.01 a	0.38 ± 0.05 c	0.92 ± 0.03 a
Mg (%)	0.20 ± 0.03 bc	0.26 ± 0.02 b	1.35 ± 0.07 a	0.08 ± 0.00 c
S (%)	0.72 ± 0.02 a	0.85 ± 0.23 a	0.04 ± 0.00 b	0.33 ± 0.02 b
Cu (mg kg^{-1})	132 ± 13.1 b	196 ± 20.2 a	51.7 ± 2.49 c	3.67 ± 0.94 d
Fe (mg kg^{-1})	24,572 ± 298 a	31,252 ± 7885 a	31,435 ± 16,974 a	22,021 ± 856 a
Mn (mg kg^{-1})	84.3 ± 15.4 b	116 ± 23.6 b	152 ± 5.19 b	1639.±38.2 a
Zn (mg kg^{-1})	436 ± 33.7 a	570 ± 84.9 a	126 ± 1.70 b	194 ± 0.82 b
K^1_{Total} (%)	0.35 ± 0.11 c	0.52 ± 0.11 c	1.73 ± 0.07 a	1.11 ± 0.20 b
K^2_{Total} (%)	-	-	3.16 ± 0.17	9.24 ± 0.65
Cd (mg kg^{-1})	2.00 ± 1.00 a	1.67 ± 0.58 a	1.67 ± 0.58 a	1.33 ± 0.58 a
Ni (mg kg^{-1})	15.0 ± 0.00 b	15.7 ± 3.21 b	54.7 ± 0.58 a	5.67 ± 1.15 c
Pb (mg kg^{-1})	34.0 ± 2.65 b	45.7 ± 2.08 a	16.7 ± 0.58 d	21.7 ± 1.53 c
N (%)	3.67 ± 0.07	2.93 ± 0.09	< L.D.	< L.D.
C (%)	22.8 ± 0.46 a	20.8 ± 0.67 b	0.59 ± 0.03 c	0.91 ± 0.03 c
H (%)	3.82 ± 0.08	2.86 ± 0.07	< L.D.	< L.D.
O (%)	22.6 ± 0.55	9,80 ± 0,58	-	-
C/N	6.26 ± 0.02	7.12 ± 0.01	-	-
H/C	0.16 ± 0.00	0.14 ± 0.00	-	-
O/C	0.99 ± 0.04	0,47 ± 0.04	-	-
VM (% bs)	45.3 ± 0.87	24.7 ± 0.16	-	-
Cinzas (% db)	47.1 ± 0.56	63.6 ± 0.19	-	-
FC (% bs)	7.51 ± 0.31	11.7 ± 0.06	-	-

Means followed by the same letters do not differ from each other according to Tukey's test ($p < 0.05$); mean ± standard deviation ($n = 3$); db: dry basis; L.D.: Limit of detection; [1] Determined by nitroperchloric extraction; [2] Determination by hydrofluoric and perchloric acid extraction. VM: volatile material, FC: fixed carbon. Adapted from Santos et al. (2026).

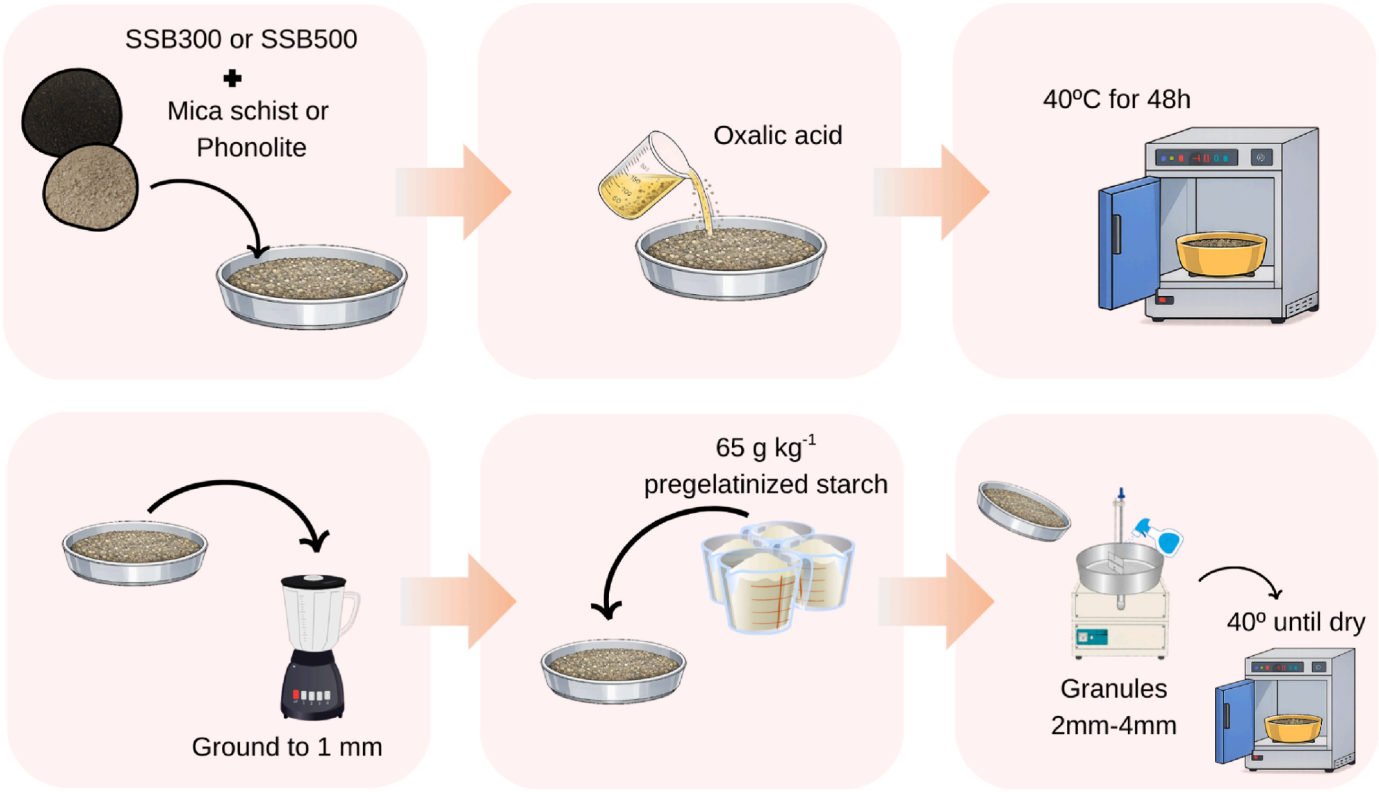

Fig. 1. Diagram showing the production steps and the composition of the raw materials used in the synthesis of fertilizers.

Table 2
Biochar-based fertilizer (BBF) formulations evaluated in the study.

Treatment code	Biochar (SSB)	Agromineral	OA (mol L^{-1})
SSB300+Mica + OA_0	300 °C	Mica schist	0
SSB300+Mica + $OA_{0.33}$	300 °C	Mica schist	0.33
SSB300+Mica + $OA_{0.67}$	300 °C	Mica schist	0.67
SSB300+Mica + OA_1	300 °C	Mica schist	1.00
SSB500+Mica + OA_0	500 °C	Mica schist	0
SSB500+Mica + $OA_{0.33}$	500 °C	Mica schist	0.33
SSB500+Mica + $OA_{0.67}$	500 °C	Mica schist	0.67
SSB500+Mica + OA_1	500 °C	Mica schist	1.00
SSB300+Phon + OA_0	300 °C	Phonolite	0
SSB300+Phon + $OA_{0.33}$	300 °C	Phonolite	0.33
SSB300+Phon + $OA_{0.67}$	300 °C	Phonolite	0.67
SSB300+Phon + OA_1	300 °C	Phonolite	1.00
SSB500+Phon + OA_0	500 °C	Phonolite	0
SSB500+Phon + $OA_{0.33}$	500 °C	Phonolite	0.33
SSB500+Phon + $OA_{0.67}$	500 °C	Phonolite	0.67
SSB500+Phon + OA_1	500 °C	Phonolite	1.00

SSB300 and SSB500: Biochar made from sewage sludge pyrolyzed at 300 and 500 °C, respectively; Mica: mica schist; Phon: phonolite; OA: oxalic acid.

and 1° min^{-1}. Minerals were identified by comparison with standards from the International Centre for Diffraction Data (ICDD). Thermogravimetric analysis (TG) was performed in an inert nitrogen (N_2) atmosphere, with a flow rate of 50 mL min^{-1}, under temperature variation from ambient to 1000 °C, in alumina crucibles, using a heating rate of 20 °C min^{-1} on a DTG-60H instrument (Shimadzu, Kyoto, Japan). Differential thermogravimetry (DTG) curves were obtained by numerical derivation of thermogravimetric (TG) curves. Fourier transform infrared (FTIR) spectroscopy of the BBFs was obtained on a KBr pellet (4000–400 cm^{-1}, 4 cm^{-1}) using a Vertex 70 spectrophotometer (Bruker, Karlsruhe, Germany).

The apparent density (AD) of the granules was determined according to British Standards Institution (1995), filling 50 cm^3 cylinders. The particle density (PD) was obtained by measuring the volume of 10 granules using a digital caliper and weighing each granule individually. The densities were calculated according to equations (1) and (2).

$$AD = \frac{w}{v} \quad (1)$$

Where, AD = apparent density (g cm^{-3}); w = weight of material needed to fill the cylinder (g); v = volume of the cylinder (cm^3).

$$PD = \frac{wg}{vg} \quad (2)$$

Where, PD = particle density of the granule (g cm^{-3}); wg = weight of the granule (g); vg = volume of the granule (cm^3).

2.4. Stability and indicators associated with potential for C sequestration

2.4.1. Production efficiency of BBFs

To accurately quantify the efficiency of BBF production, the yield and retention rate of C were calculated using equations (3) and (4) (Fei et al., 2025).

$$Production\ efficiency = \frac{Mbc}{Mss}\ x\ 100 \quad (3)$$

$$C\ retention\ rate = \frac{Mbc\ x\ Cbc}{(Mss\ x\ Css + Ma\ x\ Cad)} x100 \quad (4)$$

Where Mbc = mass of solid residue resulting from pyrolysis (g); Mss = mass of SS (g); Cbc = C content (%) of biochar; Css = C content of SS (%); Ma = mass of added minerals (g); Cad = C content of added minerals (%).

2.4.2. C stability of BBFs

The stability of C can be analyzed in several ways, and the methods are grouped into three categories: I) analysis of the C structure of biochar; II) determination of the oxidation resistance of biochar; and III)

evaluation of biochar persistence through incubation and modeling of the mineralization rate (Leng et al., 2019). In the present study, the chosen methods were selected based on their advantages and disadvantages and fell into categories I and II.

In category I, analysis of the structure of C, the elementary ratios H/C, O/C, O + N/C and the Van Krevelen diagram were used, which represents the ratio H/C as a function of O/C.

Category II, oxidative resistance, was analyzed through thermal stability (TSF) using proximate analysis and the VM/FC (Cely et al., 2015) (Equation (5)) and TG relationships using the recalcitrance index (R_{50}) (Harvey et al., 2012) (Equation (6)).

$$TSF = \frac{FC}{(VM\ x\ FC)}\ x\ 100 \tag{5}$$

Where FC = fixed C, VM = volatile material.

$$R_{50} = \frac{T_{50,BBF}}{T_{50,graphite}} \tag{6}$$

Where $T_{(50,\ BBF)}$ = temperature corresponding to a 50% oxidation of BBF, while $T_{(50,\ graphite)}$ = temperature at which 50% oxidation of graphite occurs.

2.4.3. Indicators associated with potential for C sequestration

A ternary diagram with the information obtained through proximate analysis (VM, FC and ash) was one of the methodologies used to analyze the C sequestration potential.

Additionally, the C sequestration potential was calculated based on the final amount of C that would remain sequestered in the soil. Deducting the C lost during pyrolysis from the initial C in the gross biomass and then multiplying by the C recalcitrance (R_{50}) (Zhao et al., 2013 adapted) (Eq. (7)).

$$Potential\ for\ C\ sequestration = \frac{Mbbf\ x\ \%BC\ x\ Cbbf\ x\ R_{50}}{Mss\ x\ Css}\ x\ 100 \tag{7}$$

Where, Mbbf = mass of BBF (g), Cbbf = C content of BBF, % BC = percentage of biochar in the fertilizer formulation, Mss = mass of SS, Css = C of SS and R_{50} = recalcitrance index.

2.5. Statistical analysis

The data were obtained in triplicate and initially analyzed for normality of residuals and homoscedasticity of variance according to Shapiro-Wilk and Levene tests, respectively, at a significance level of 5%. Subsequently, the data were subjected to analysis of variance (ANOVA), and the means were compared using Tukey's test ($P < 0.05$). Additionally, the data obtained were subjected to principal component analysis (PCA). All analyses were performed using IBM SPSS Statistics software.

3. Results and discussion

3.1. Physical-chemical and mineralogical characteristics of fertilizers

The pH of the BBFs was influenced by the combination of materials used in fertilizer production, ranging from 4.07 to 5.97 (Table 3). Despite the statistical differences observed between some treatments, the overall variation was low, with values within the soil pH range considered suitable for agricultural cultivation, between 5.4 and 6.4 (Malavolta, 2006). In comparison, conventional fertilizers have a wide pH range, from very acidic, such as triple superphosphate (pH 3.1), urea phosphate (pH 2.7) and ammonium sulfate (pH 4.0), to neutral or alkaline materials, such as dicalcium phosphate (pH 7.0), urea (pH 7.6) and sodium nitrate (pH 9.6) (Trani and Trani, 2011). In the present study, the new BBFs exhibited pH values in the intermediate to moderate range (between 4 and 6), avoiding both extreme acidity and high

Table 3
Chemical properties of biochar-based fertilizers with silicate agrominerals in different concentrations of oxalic acid.

Fertilizers	pH	P (%)	K (%)	N (%)	Ca (%)	Mg (%)	S (%)	Volatile material (%bs)	Ashes (%db)	Fixed C (%db)
SSB300+Mica + OA_0	5.87 ± 0.54a	1.56 ± 0.14a	0.65 ± 0.04a	1.60 ± 0.04de	0.54 ± 0.01cd	0.11 ± 0.02a	0.60 ± 0.02a	23.79 ± 0.07h	72.81 ± 0.12b	3.40 ± 0.12e
SSB300+Mica + $OA_{0,33}$	4.87 ± 0.31b	1.59 ± 0.11a	0.70 ± 0.07a	1.59 ± 0.03de	0.49 ± 0.07cd	0.09 ± 0.01a	0.57 ± 0.02 ab	26.90 ± 0.63f	69.87 ± 0.56d	3.23 ± 0.25e
SSB300+Mica + $OA_{0,67}$	4.07 ± 0.05c	1.56 ± 0.02a	0.61 ± 0.02a	1.25 ± 0.03 fg	0.50 ± 0.05cd	0.12 ± 0.03a	0.51 ± 0.03b	28.08 ± 0.27f	68.57 ± 0.14e	3.36 ± 0.13e
SSB300+Mica + OA_1	5.27 ± 0.37 ab	1.51 ± 0.16a	0.63 ± 0.02a	1.20 ± 0.06gh	0.43 ± 0.00d	0.11 ± 0.01a	0.55 ± 0.01 ab	30.95 ± 0.86e	65.43 ± 0.94f	3.62 ± 0.13e
SSB500+Mica + OA_0	5.53 ± 0.12 ab	1.69 ± 0.08a	0.66 ± 0.04a	1.01 ± 0.03hi	0.52 ± 0.10cd	0.10 ± 0.01a	0.54 ± 0.03 ab	17.51 ± 0.15j	78.10 ± 0.19a	4.39 ± 0.09d
SSB500+Mica + $OA_{0,33}$	5.73 ± 0.09a	1.69 ± 0.08a	0.65 ± 0.04a	1.00 ± 0.03i	0.49 ± 0.03cd	0.13 ± 0.02a	0.54 ± 0.04 ab	21.80 ± 0.13i	73.88 ± 0.19b	4.32 ± 0.13d
SSB500+Mica + $OA_{0,67}$	5.50 ± 0.08 ab	1.53 ± 0.06a	0.60 ± 0.01a	0.90 ± 0.07i	0.52 ± 0.02cd	0.12 ± 0.01a	0.56 ± 0.04 ab	24.08 ± 0.19gh	71.55 ± 0.23c	4.37 ± 0.04d
SSB500+Mica + OA_1	5.60 ± 0.08 ab	1.72 ± 0.10a	0.62 ± 0.04a	0.89 ± 0.07i	0.50 ± 0.05cd	0.13 ± 0.01a	0.58 ± 0.02 ab	25.30 ± 0.09g	70.34 ± 0.19cd	4.35 ± 0.13d
SSB300+Phon + OA_0	5.57 ± 0.21 ab	1.86 ± 0.16a	0.28 ± 0.00b	2.12 ± 0.08a	0.76 ± 0.07bc	0.10 ± 0.01a	0.55 ± 0.02 ab	36.86 ± 0.11c	56.24 ± 0.21i	6.89 ± 0.16c
SSB300+Phon + $OA_{0,33}$	5.73 ± 0.17a	1.59 ± 0.11a	0.26 ± 0.02b	2.02 ± 0.07 ab	0.79 ± 0.18bc	0.12 ± 0.02a	0.55 ± 0.00 ab	38.80 ± 0.24b	54.46 ± 0.21j	6.74 ± 0.05c
SSB300+Phon + $OA_{0,67}$	5.87 ± 0.12a	1.95 ± 0.14a	0.26 ± 0.02b	1.81 ± 0.09c	0.57 ± 0.04cd	0.13 ± 0.01a	0.61 ± 0.02a	39.60 ± 0.14b	53.95 ± 0.13j	6.45 ± 0.09c
SSB300+Phon + OA_1	5.80 ± 0.08a	1.85 ± 0.14a	0.30 ± 0.04b	1.83 ± 0.04bc	0.68 ± 0.05bcd	0.12 ± 0.02a	0.57 ± 0.02 ab	41.09 ± 0.34a	52.40 ± 0.31k	6.51 ± 0.03c
SSB500+Phon + OA_0	5.90 ± 0.08a	1.92 ± 0.09a	0.40 ± 0.06b	1.64 ± 0.01cd	0.93 ± 0.06b	0.14 ± 0.01a	0.58 ± 0.01 ab	24.87 ± 0.13gh	66.32 ± 0.15f	8.81 ± 0.15a
SSB500+Phon + $OA_{0,33}$	5.80 ± 0.08a	1.95 ± 0.14a	0.27 ± 0.00b	1.53 ± 0.03de	0.63 ± 0.03bcd	0.13 ± 0.01a	0.60 ± 0.02a	30.92 ± 0.44e	60.95 ± 0.23g	8.13 ± 0.47b
SSB500+Phon + $OA_{0,67}$	5.97 ± 0.09a	1.85 ± 0.14a	0.38 ± 0.14b	1.55 ± 0.02de	0.81 ± 0.04bc	0.12 ± 0.01a	0.58 ± 0.02 ab	32.65 ± 0.06d	59.71 ± 0.20h	7.65 ± 0.14b
SSB500+Phon + OA_1	5.80 ± 0.08a	1.91 ± 0.10a	0.35 ± 0.00b	1.43 ± 0.04ef	1.42 ± 0.22a	0.14 ± 0.01a	0.58 ± 0.00 ab	30.92 ± 0.18e	61.23 ± 0.16g	7.85 ± 0.03b

Means followed by the same letters do not differ from each other by Tukey's test ($p < 0.05$); mean ± standard deviation (n = 3). SSB: sewage sludge biochar produced at 300 °C (SSB300) and 500 °C (SSB500); Mica: mica schist; Phon: phonolite; OA: oxalic acid in different concentrations (mol L^{-1}); db: dry basis.

alkalinity, which can compromise nutrient availability or cause toxicity in plants. Controlling acidity through active ingredients in formulations offers a significant advantage, as it enables pH control, which is difficult to achieve with conventional fertilizers that have a fixed pH.

Regarding primary macronutrients (Table 3), P was balanced among the BBFs (1.51–1.95%), not being affected by the type of agromineral or pyrolysis temperature. On the other hand, K was dependent on the ASi, with higher concentrations in mixtures with Mica (0.60–0.70%) and lower concentrations with Phon (0.26–0.40%), reflecting the specific mineralogical characteristics. Certain minerals have satisfactory concentrations of K, but this element is associated with different mineral structures. Phon has microcline and muscovite, while Mica has muscovite and biotite (Fig. S1B). Muscovite and biotite are 2:1 mineral structures, in which K links tetrahedral and octahedral layers; in muscovite, these layers contain Si and Al, conferring greater stability and low availability; In biotite, Si and Mg/Fe promote lower stability and higher availability (Krahl et al., 2022a). Microcline, on the other hand, presents K strongly integrated into the tetrahedral network of SiO_4 and AlO_4, in a 3:1 ratio, forming a resistant structure that requires intense weathering for K release (Melo and Alleoni, 2019), which directly influences the availability of this nutrient to plants. N stood out in formulations with Phon and SSB300 (1.83–2.12%), a result of the higher proportion of SSB combined with the characteristic of SSB300 having a higher content of oxygenated and nitrogenous groups (Aktar et al., 2022).

Among the secondary macronutrients (Table 3), Ca had the highest concentration in BBFs with Phon, reaching up to 1.42% in SSB500+Phon + OA_1, while Mg (0.09% – 0.14%) and S (0.51% to 0.61%) showed little variation, indicating a balance between the formulations. Among the micronutrients (Table S1), Cu was more concentrated in mixtures with SSB500, Fe predominated in mixtures with Mica (greater than 30,000 mg kg^{-1}), Mn had the highest concentration in mixtures with Phon (up to 330 mg kg^{-1}), and Zn remained balanced (209 mg kg^{-1} – 396 mg kg^{-1}). All these characteristics result from the concentrations of the raw materials in each formulation. This creates potential for formulations that can be used in crops with higher demands for various macro- and micronutrients (Santos et al., 2026).

For the C and H contents (Table S1), the highest values ($p < 0.05$) were observed in the SSB300+Phon + OA treatments (0, 0.33, 0.67 and 1 mol L^{-1}), ranging from 18.7 to 19.2% for C and from 1.77 to 2.10% for H, indicating that the use of Phon associated with biochar produced at 300 °C promoted greater incorporation of C and hydrogenated compounds, regardless of the addition of OA. Similarly, for the O content, the highest averages ($p < 0.05$) were observed in the SSB300+Phon + OA treatments (0.33, 0.67 and 1 mol L^{-1}), with values between 22.3 and 24.0%. These results indicate a high abundance of oxygenated functional groups in these BBFs, which may be associated with increased polarity and surface reactivity in soil (Yi et al., 2025).

Higher mean values ($p < 0.05$) for moisture, VM, ash, and FC (Table 3) were observed for the biochars SSB500+Phon + OA_1, SSB300+Phon + OA_1, SSB500+Mica + OA_0, and SSB500+Phon + OA_0, respectively. The high ash content in SSB500+Mica + OA_0 is associated with the high ash content of the SSB500 biochar (63.6%; Table 1), resulting from pyrolysis at a higher temperature, in which the volatilization of the organic fraction promotes the concentration of inorganic components, favoring enrichment in mineral elements such as Ca, Mn, Zn, and P (Figueiredo et al., 2018)

Regarding potentially toxic elements (Table S1), Cd concentrations in the fertilizers were low, ranging from 1 to 6 mg kg^{-1}. Pb levels ranged from 28 mg kg^{-1} to 53.67 mg kg^{-1}, while Ni levels ranged from 33.33 mg kg^{-1} to 73 mg kg^{-1}. It should be noted that the reported values refer to total concentrations and do not directly correspond to the available or bioavailable fractions. All values met the limits established for organomineral fertilizers (Brasil, 2006), except for the SSB500+Mica + OA_0 treatment, which presented 73 mg kg^{-1} of Ni, exceeding the maximum limit allowed by Brazilian legislation (70 mg kg^{-1}). However, Ni, despite being considered a potentially toxic element, is also essential for plants; it is a component of urease, and its deficiency results in necrotic lesions on leaves due to toxic accumulation of urease (Dalton, 1988; Kabata-Pendias, 2000). Furthermore, this small excess of Ni can be corrected by adjusting the BBF formulation, reducing the mica fraction, which has the highest Ni concentration among those evaluated (Table 1).

According to energy-dispersive X-ray spectroscopy (EDX), the most representative elements in the formulations reflect the nature of the ASi and SSB used. Al and Si concentrations were the most representative (Fig. S2 and Table S2), with the Al portion originating mainly from the SSBs and the Si portion from the minerals (Mica and Phon) (Fig. S1A). P and Ca contents were mostly derived from the SSBs (Fig. S1A). Formulations with SSB500 showed higher concentrations of P (up to 14.7%) and Ca (up to 4.3%) (Table S2). This higher concentration results from the decomposition and loss of organic matter, as well as the retention of stable inorganic components during pyrolysis (Figueiredo et al., 2021; Makowska et al., 2025). Therefore, the role of SSB as the main source of these essential nutrients stands out, while ASi contribute mainly with the macronutrients K and Mg and micronutrients such as Fe (Fig. S1A).

The concentration of K, a key element in the K rocks used, showed clear differences between the types of ASi (Fig. S2 and Table S2). Fertilizers with Mica contained 3.8%-4.3% K, whereas those with Phon had higher concentrations of 4.7%-5.9%, indicating that the choice of ASi is crucial for K supply. However, this result differs from that obtained in the chemical analysis (Table 3), in which fertilizers with Mica showed higher K values than those formulated with Phon. This is due to the analytical technique used in each analysis. EDX analysis has limitations in identifying light elements, detecting only those with an atomic number of 11 or higher (Na to U), which prevents quantification of H, C, N, and O. In contrast, chemical analysis depends on the extraction of elements by solubilization, the efficiency of which can vary according to the nature of the chemical bonds present (Santos et al., 2026). It is also noteworthy that the chemical analysis of K was performed using nitroperchloric acid digestion (Brasil, 2017), which is intended for organomineral fertilizers and does not reach more complex silicate structures, such as the microcline present in Phon, thereby generating underestimated values. The variation in OA concentration in the formulation did not induce significant changes in the basic elemental composition detected by EDX, suggesting that the acidifying agent acts preferentially on nutrient solubilization and release, as evidenced by previous studies Lustosa Filho et al. (2026) and Santos et al. (2026).

XRD analysis of the fertilizers showed a predominance of mineral phases derived from the raw materials, with no formation of new potassium crystalline phases (Fig. 2). In the BBF samples with Mica, quartz (SiO_2), muscovite [$KAl_2(AlSi_3O_{10})(OH)_2$] and biotite [$K(Mg,Fe)_3AlSi_3O_{10}(OH)_2$] were identified, in addition to berlinite ($AlPO_4$) associated with the P of the SSB (Santos et al., 2026). In general, there was a reduction in the intensity of the peaks associated with SSB in the materials in the presence of OA, indicating the action of the acid on the SSB. In formulations with Phon, microcline ($KAlSi_3O_8$) was the dominant phase, maintaining high structural stability even with the addition of OA, highlighting the low reactivity of this material.

The TG/DTG curves show multiple mass-loss events associated with the thermal decomposition of the organic and mineral constituents of the fertilizers (Fig. 3 and Table S3). The initial mass losses up to ~200 °C, common to all samples, are primarily attributed to the removal of adsorbed water and the degradation of OA. Oxalic acid decomposes into C monoxide, CO_2, and water at 100 °C (Riemenschneider and Tanifuji, 2011). A greater mass reduction is observed in samples with higher OA concentrations (6.47% to 9.37%), as confirmed by the higher intensity of the DTG peaks in fertilizers with higher OA levels. Between 200 and 400 °C, the main mass loss stage occurs, most pronounced in samples produced with SSB300 (11.67% to 19.79%), due to the higher content of thermally unstable organic matter from pyrolyzed sludge at 300 °C (Aktar et al., 2022; Mbasabire et al., 2024), associated with the

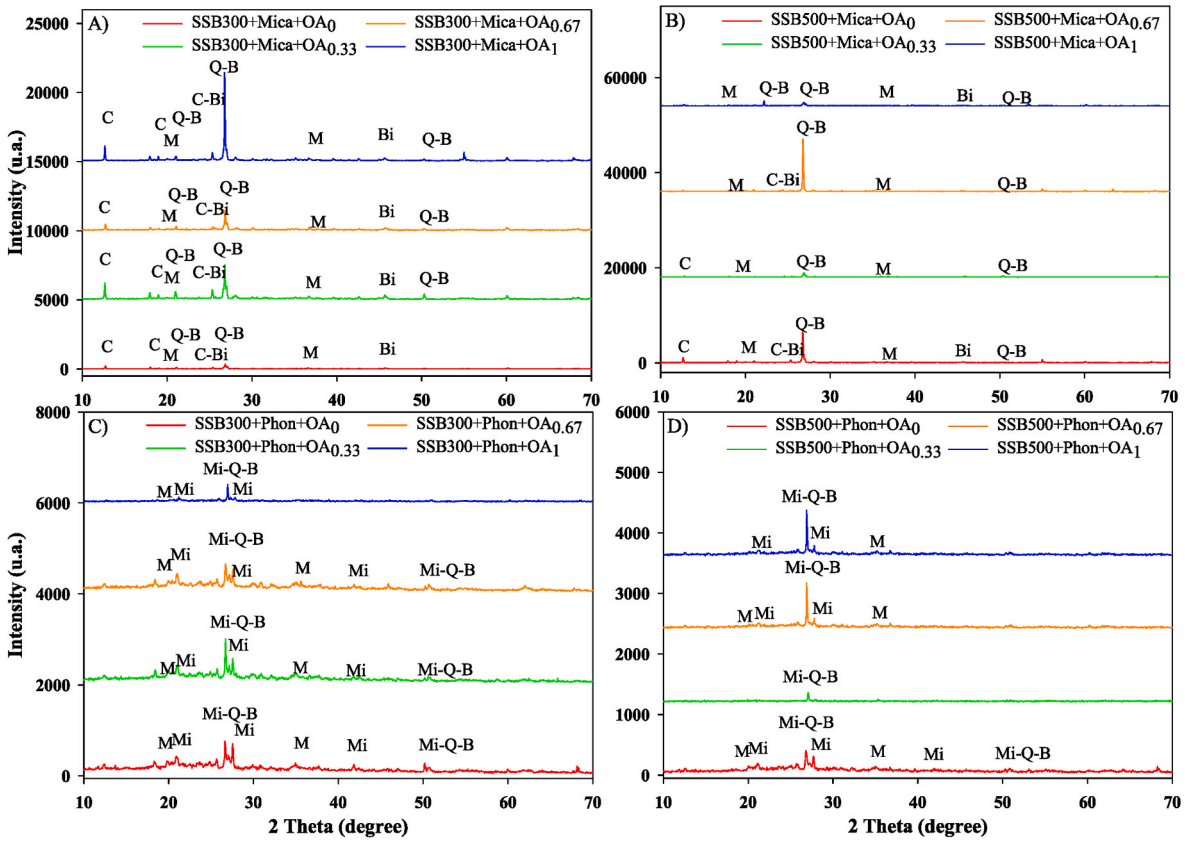

Fig. 2. XRD spectra of sewage sludge biochar-based fertilizers, mica schist (Mica) or phonolite (Phon) subjected to different concentrations of oxalic acid (OA). (A) SSB300+Mica; (B) SSB500+Mica; (C) SSB300+Phon; and (D) SSB500+Phon, each under OA concentrations of 0, 0.33, 0.67, and 1.00 mol L^{-1}. B: berlinite; Bi: biotite; C: clinochlore; M: muscovite; Mi: microcline; Q: quartz.

decomposition of the starch used as a binder. The influence of OA is also observed, since samples with higher concentrations of this agent showed a greater mass reduction in this temperature range (SSB300+Mica + OA_1: 14.62% and SSB300+Phon + OA_1: 19.79%). The formulations with SSB500 stand out, further widening the difference between fertilizers with and without OA, indicating a stronger interaction of the acid with the C chain of SSB500 (Table S3). The presence of OA in BBF promotes the formation of new functional groups, resulting in a more chemically functionalized material (Lustosa Filho et al., 2026), which, in turn, may promote partial disruption and instability in the C structures. Above 400–500 °C, losses become more gradual and are associated with the decomposition of more recalcitrant organic residues, being less pronounced in samples with SSB500, which exhibit greater thermal stability due to the greater aromaticity of C (Aktar et al., 2022). Formulations with Phon, characterized by a higher proportion of SSB (725 g) and a lower proportion of ASi, exhibit more pronounced mass losses throughout the period, reflecting lower stability (Table S3). Thus, both the pyrolysis temperature and the relative proportions of SSB, ASi, and OA control the thermal stability and decomposition behavior of these organomineral fertilizers. This reinforces the combined effect of pyrolysis and OA on the thermal behavior and structural reactivity of these BBFs.

FTIR spectroscopy revealed significant changes in the functional groups of fertilizers as a function of pyrolysis temperature, ASi type, and OA concentration (Fig. 4). In all samples, a broad band between 3600 and 3000 cm^{-1} was observed, attributed to O–H and N–H stretching vibrations, related to hydroxyl groups, starch, and organic sludge residues, being more intense in formulations with SSB300, due to the higher content of thermally unstable oxygenated and nitrogenated groups (Aktar et al., 2022; Antunes et al., 2017; Raj et al., 2021). The bands at ~2920 cm^{-1} and 2850 cm^{-1} corresponding to aliphatic C–H (CH_2 and CH_3) are more pronounced in samples pyrolyzed at 300 °C and decrease significantly at 500 °C, indicating spectral features consistent with increased aromatization and condensation of C with increasing pyrolysis temperature (Aktar et al., 2022; Mbasabire et al., 2024). The region between 1750 cm^{-1} – 1600 cm^{-1} shows bands attributed to C=O and C–O of carboxylic and carbonyl groups, whose intensity increases progressively with the addition of OA (0.33 to 1 mol L^{-1}). Bands in the 1200 cm^{-1}–900 cm^{-1} range, associated with C–O and Si–O, reflect the contribution of silicate phases from ASi and SSBs and show less variation with the addition of OA, being more defined in samples with Phon, due to the predominance of microcline (Liu et al., 2021; Lonappan et al., 2020; Rehman et al., 2020), while pyrolysis at 500 °C results in structurally more stable materials with a lower density of surface functional groups(Figueiredo et al., 2018; Raj et al., 2021; Yuan et al., 2015).

The apparent density (AD) of the fertilizers ranged from 0.52 to 0.80 g cm^{-3}, while the particle density (PD) ranged from 1.02 to 1.54 g cm^{-3}, showing that both the pyrolysis temperature of SS and the type of agromineral added (Mica or Phon) and the concentration of OA affected the physical properties of the fertilizers (Fig. S3). In general, AD increased with increasing OA concentration, especially between 0.67 mol L^{-1} and 1 mol L^{-1}, and these values differed ($p < 0.05$) from those of treatments with lower concentrations or without OA. This behavior suggests that the acid treatment favored particle compaction and rearrangement, possibly due to the solubilization of mineral phases followed by their subsequent precipitation (Santos et al., 2026), even at low concentrations that were not detected by XRD analysis (Fig. 2). The BBFs did not show a clear pattern of PD response to increased OA concentration, with no statistically significant effect attributable to the acid. Comparatively, fertilizers formulated with Mica showed a higher PD (1.41 g cm^{-3}) than those containing Phon (1.17 g cm^{-3}), reflecting differences in formulation proportions, mineralogical composition, and

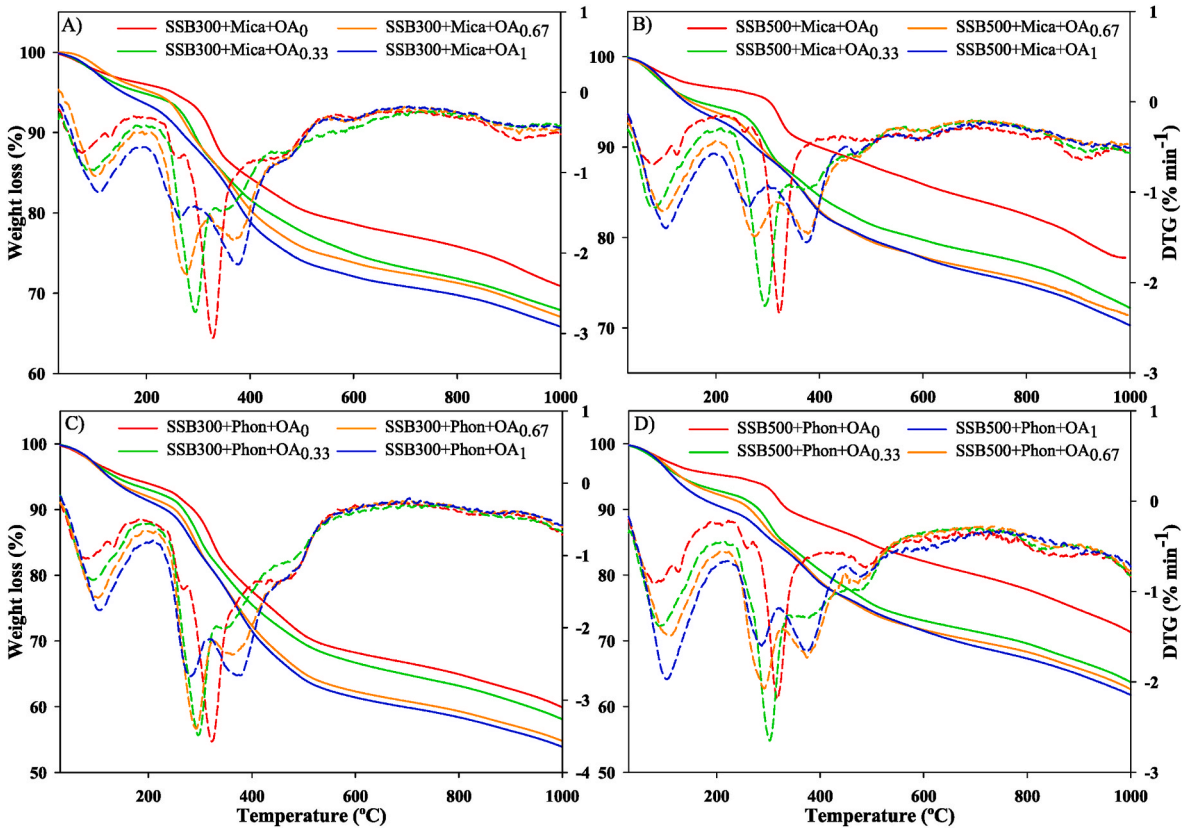

Fig. 3. Thermogravimetric (TG) (solid line) and differential thermogravimetric (DTG) (dashed line) analyses of sewage sludge biochar-based fertilizers (SSB), mica schist (Mica) or phonolite (Phon) subjected to different concentrations of oxalic acid (OA). (A) SSB300+Mica; (B) SSB500+Mica; (C) SSB300+Phon; and (D) SSB500+Phon, each under OA concentrations of 0, 0.33, 0.67, and 1.00 mol L^{-1}.

the interaction between SSB and added Asi.

Taken together, the results of the chemical, elemental, mineralogical, and spectroscopic analyses indicate that the properties of the BBFs are governed by interactions between pyrolysis temperature, agromineral type, oxalic acid (OA) addition, and formulation ratio. Pyrolysis temperature regulates the C structure, as evidenced by elemental ratios (H/C and O/C), FTIR, and TG analyses. Materials produced at 500 °C exhibit greater aromaticity and thermal stability, whereas those produced at 300 °C retain a higher abundance of functional groups, increasing their reactivity. Similar temperature-dependent trends were reported by Santos et al. (2026) for OA-activated SSBs, with lower pyrolysis temperatures enhancing nutrient reactivity and higher temperatures promoting greater aromaticity and structural stability of the C matrix. The agrominerals define the K reservoir, as indicated by XRD and EDX, with availability depending on the structural organization of silicates. Microcline, with a 3:1 silicate framework, is more resistant, whereas biotite and muscovite, with 2:1 silicate structures, are more susceptible to acid attack (Krahl et al., 2022a, 2022b; Melo and Alleoni, 2019; Santos et al., 2026).

In this context, OA serves as both an acidifying and complexing agent, probably promoting simultaneous changes in mineral and organic phases. The increased reactivity observed in OA-treated formulations aligns with previous studies showing that OA enhances mineral dissolution through acidification and cation complexation (Awoniyi et al., 2025). OA dissociation releases protons that promote mineral dissolution and functional-group transformations, while oxalate anions act as ligands, forming stable complexes with cations such as Al^{3+}, Fe^{3+}, and Ca^{2+}. This process removes cations from the mineral surface, shifts the reaction equilibrium, and sustains dissolution, characterizing a ligand-controlled dissolution mechanism and highlighting kinetics that depend on acid concentration and mineral reactivity (Dabare and Munaweera, 2026). This is supported by reduced peak intensity in XRD patterns for SSB500+Mica and SSB300+Phon formulations, increased mass loss in TG, and changes in functional groups observed by FTIR, particularly the emergence of C–O and C=O groups associated with carboxylic acids.

At the molecular level, OA dissociation releases protons that can protonate biochar surface groups ($\equiv C–O^- + H^+ \rightarrow \equiv C–OH$), a process that tends to be more pronounced in SSB300-based formulations due to their higher content of oxygenated functional groups (Aktar et al., 2022), as indicated by elemental ratios and FTIR analyses. These protons also promote the cleavage of Si–O–K bonds in minerals ($\equiv Si–O–K + H^+ \rightarrow \equiv Si–OH + K^+$), releasing cations. Simultaneously, oxalate ($C_2O_4^{2-}$) forms complexes with these cations, reducing their activity in solution and thereby enhancing mineral dissolution (Santos et al., 2026). This behavior aligns with recent studies showing that OA promotes both proton-assisted and ligand-controlled dissolution mechanisms in K-bearing silicate minerals, particularly in mica structures, which are generally more susceptible to weathering than feldspathic minerals (Awoniyi et al., 2025). Additionally, OA can act on phosphorus in the SSB. XRD data show a reduction in the intensity of berlinite ($AlPO_4$) peaks with increasing OA concentration, indicating its dissolution under acidic conditions ($AlPO_4 + 3H^+ \rightarrow Al^{3+} + H_3PO_4$). Concurrently, the released Al^{3+} reacts with oxalate to form poorly soluble aluminum oxalate ($2Al^{3+} + 3C_2O_4^{2-} \rightarrow Al_2(C_2O_4)_3$) (Santos et al., 2026), which reduces its activity and favors continuous P dissolution.

However, this same complexation mechanism may also increase the mobility of potentially toxic elements. Although Vause et al. (2018) identified OA as the low-molecular-weight organic acid with the greatest capacity to mobilize metals, Santos et al. (2026) demonstrated that OA can maximize the release of essential nutrients, such as P, K, and Ca, without causing excessive release of toxic elements. This behavior can

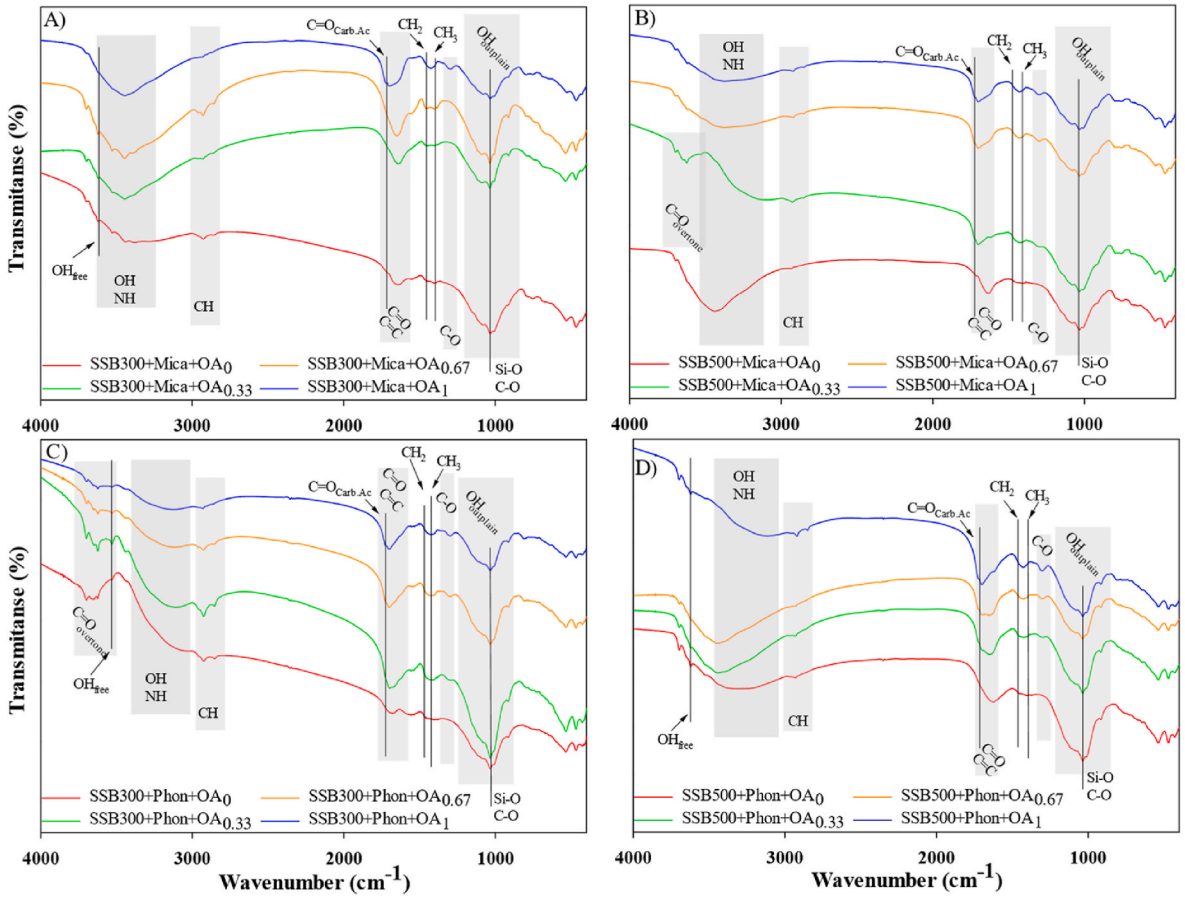

Fig. 4. FTIR spectra of sewage sludge biochar-based fertilizers (SSB), mica schist (Mica) or phonolite (Phon) subjected to different concentrations of oxalic acid (OA). (A) SSB300+Mica; (B) SSB500+Mica; (C) SSB300+Phon; and (D) SSB500+Phon, each under OA concentrations of 0, 0.33, 0.67, and 1.00 mol L^{-1}.

be explained by the nature of SS, a highly heterogeneous material whose composition varies according to the industrial profile of its source regions. In this context, SS derived from predominantly domestic effluents, as in the present study, tends to contain lower concentrations of potentially toxic elements (Kominko et al., 2024). Furthermore, a long-term field study showed that SSB produced at 300 °C and 500 °C did not significantly increase the bioavailability of potentially toxic elements (Cd, Cr, Ni, and Pb) in soil over a five-year period, while still promoting residual agronomic benefits through increased availability of essential micronutrients such as Cu, Mn, and Zn (Chagas et al., 2021).

3.2. Stability and indicators associated with potential C sequestration of fertilizers

3.2.1. Production efficiency and C retention rate of BBFs

The efficiency of SSB production was influenced by pyrolysis temperature ($p < 0.05$). SSB300 showed higher efficiency, with an average yield of approximately 73%, whereas SSB500 showed a lower yield of approximately 60% (Fig. S4). This reduction in efficiency with increasing temperature is associated with the greater intensity of thermal decomposition and volatilization processes of organic compounds, resulting in greater mass losses during pyrolysis (Figueiredo et al., 2018; Raj et al., 2021; Řimnáčová et al., 2024).

The C retention rate showed a trend similar to that of biochar production efficiency (Table S4). BBFs containing SSB300 showed the highest C retention values, ranging from 78% to 82%, regardless of the addition of Mica or Phon and the OA concentrations (0; 0.33; 0.67 and 1 mol L^{-1}), compared to those with SSB500, which had values between 58% and 62%. Carbon retention was not affected by the type of ASi or the OA concentrations. In biochars with low mineral content, increasing pyrolysis temperature increases C content (Keiluweit et al., 2010). On the other hand, in mineral-rich materials such as SSB, a decrease in C content is observed because mineral enrichment overrides carbonization (Li et al., 2018).

3.2.2. Indicators of C stability

As previously described, the greatest influence on C retention in fertilizers came from SSBs, since the minerals used to enrich fertilizers nutritionally are silicate rather than carbonate. The effectiveness of C sequestration depends directly on its stability and resistance to decomposition (Zhang et al., 2026). Thus, stability and C sequestration potential analyses were performed based on biochar methodologies. Using Structural Analysis of C (I) and Oxidative Resistance (II) (Leng et al., 2019).

3.2.2.1. Analysis of the structure of C. Atomic ratios O/C, H/C, and (O + N)/C are widely used as indicators of chemical structure, aromaticity, and C stability in biochars (Leng et al., 2019; Min et al., 2022). In general, in the present study, the H/C values of the BBFs indicate the degree of aromaticity and structural condensation, while the O/C and (O + N)/C ratios indicate the degree of polarity and hydrophobicity (Costa et al., 2025; Pariyar et al., 2020; Schreiter et al., 2018). Considering only the production of SSBs relative to SS, the O/C and (O + N)/C ratios decrease as pyrolysis temperature increases, which is associated with the formation of more complex aromatic C structures (Spokas, 2010). There are higher H/C ratios in formulations with SSB pyrolyzed at 300 °C than in formulations with SSB500, also indicating a higher degree of aromaticity in formulations with SSB500 than with SSB300.

In BBFs with mica, the SSB-to-ASi ratio was approximately 1:1, whereas in treatments with Phon, a higher SSB-to-agromineral ratio (approximately 3.5:1) was observed. This difference in composition directly influenced the elemental and structural composition of the resulting fertilizers. However, in addition to this influence, the pyrolysis temperature of the biochar and the acids directly influenced the elemental composition of the BBFs.

Fertilizers containing SSB300 generally showed higher O/C values (Fig. 5A), ranging from 1.2 to 1.5, indicating greater incorporation of O into the C structure and a greater abundance of oxygenated functional groups. These values reflect a less condensed, more polar, and potentially more reactive C structure. In contrast, BBFs with SSB500 showed lower O/C ratios (Fig. 5A), with values ranging from 0.85 to 1.2, indicating greater O loss and a higher degree of structural condensation of C. This reduction in the O/C ratio is consistent with the formation of more aromatic and hydrophobic structures, associated with greater potential resistance to chemical and biological degradation (Spokas, 2010). These results confirm the structures identified by FTIR analysis (Fig. 4).

The H/C ratio further supports this trend (Fig. 5B). Fertilizers produced with SSB300 showed higher H/C values (0.10 – 0.12), indicating a higher proportion of H bound to C and, therefore, a lower degree of aromaticity. On the other hand, BBFs produced with SSB500 showed significantly lower H/C values (0.02 – 0.06), characterizing a more aromatic and structurally stable C. H/C values below 0.4 indicate highly aromatic and stable biochars (Adhikari et al., 2024; Costa et al., 2025), reinforcing the greater stability of SSB500 compared to SSB300. This increased aromaticity and structural condensation suggest that BBFs produced with SSB at 500 °C may present greater persistence in soil, owing to increased resistance to microbial and chemical decomposition (Li and Chen, 2018).

The (O + N)/C ratio showed intermediate behavior (Fig. 5C). However, it was consistent with the other structural indicators. BBFs with SSB300 showed higher values (1.3 – 1.5), suggesting a greater presence of functional groups containing O and N, which increase the chemical reactivity of C. In contrast, treatments with SSB500 showed lower (O + N)/C values (0.95 – 1.3), indicating reduced surface functionalization and greater C condensation.

Higher concentrations of OA generated an increase in O/C and (O + N)/C ratios, indicating the addition of carboxylic functional groups, originating from OA, to the SSB structure. This reduced its stability compared to fertilizers without the acid. In fertilizers with higher Mica content, the increase in acid concentration led to more pronounced changes in the H/C and (O + N)/C ratios. In contrast, in treatments with Phon, the higher proportion of SSB seems to have attenuated this effect.

The distribution of samples in the Van Krevelen diagram (Fig. 6) may indicate the combined influence of pyrolysis temperature and fertilizer composition. Biochars produced at 500 °C without OA shifted toward lower H/C and O/C, associated with greater aromaticity and C stability. On the other hand, fertilizers with SSB300, especially those with a higher concentration of OA, are concentrated in regions indicative of lower structural condensation, reflecting the greater influence of pyrolysis temperature and OA concentration in the mixture. Thus, the results suggest that the stability of C in SS biochars is influenced not only by pyrolysis temperature but also by the relative proportions of the organic (SSB) and mineral (ASi) phases, as well as by the intensity of acid treatment. Fertilizers with a higher mineral proportion, higher pyrolysis temperature, and lower OA concentration favor the formation of more aromatic and stable C structures, while fertilizers with a higher

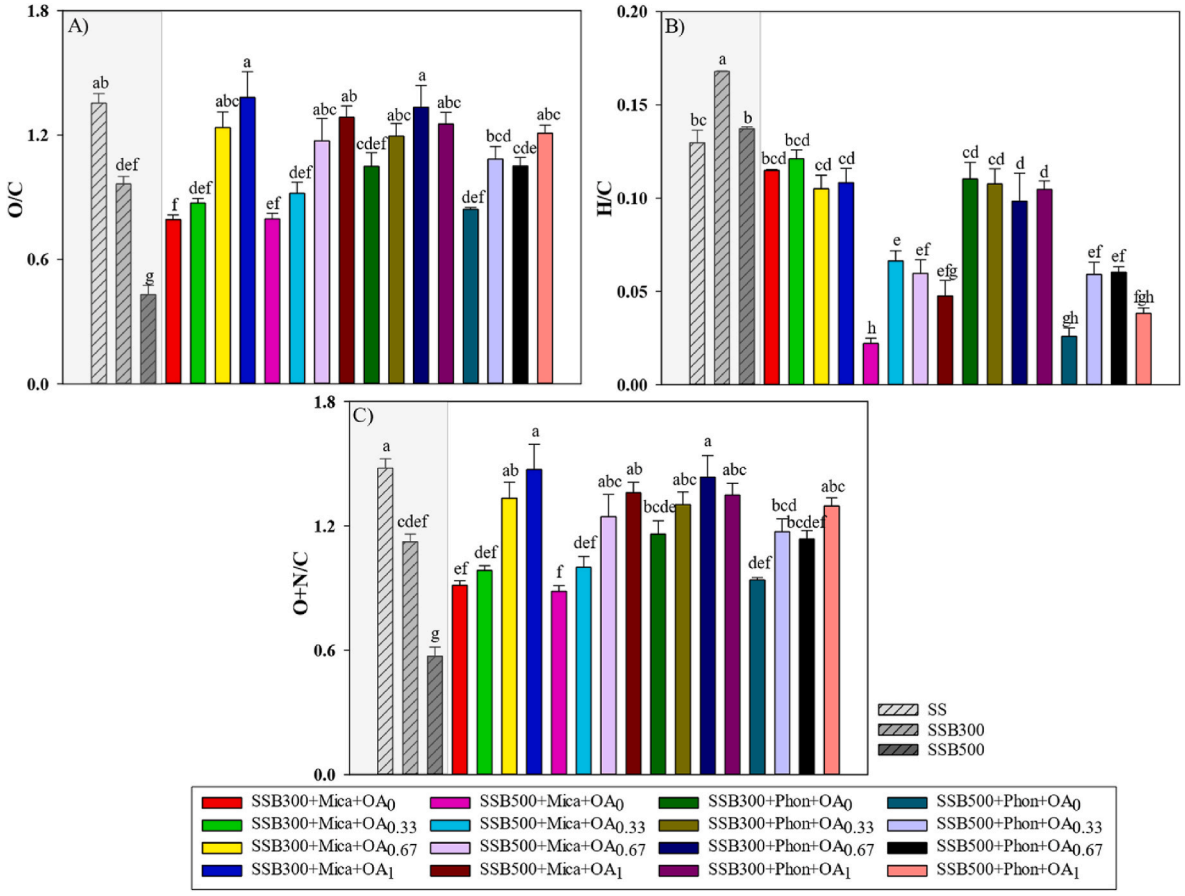

Fig. 5. Elemental ratios (A) O/C, (B) H/C and (C) O + N/C of sewage sludge (SS), pyrolyzed sewage sludge biochar at 300 °C and 500 °C (SSB300 and SSB500) and sewage sludge biochar-based fertilizers (SSB), mica schist (Mica) or phonolite (Phon) subjected to different concentrations of oxalic acid (OA). Different letters indicate significant differences among treatments according to Tukey's test ($p < 0.05$).

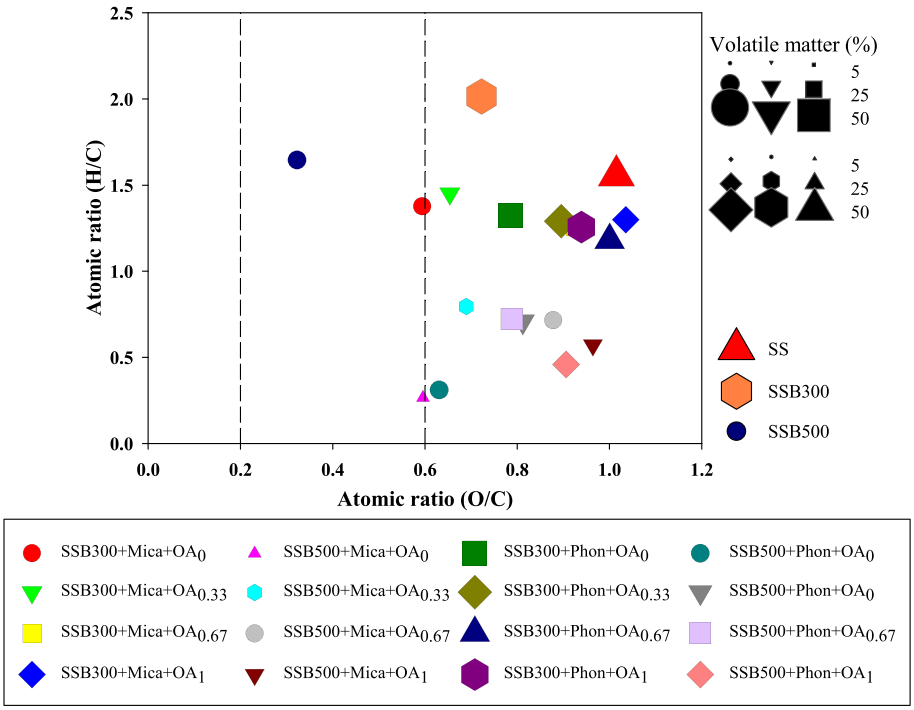

Fig. 6. Van Krevelen diagram of sewage sludge biochar-based fertilizers (SSB), mica schist (Mica) and phonolite (Phon) subjected to different concentrations of oxalic acid (OA).

SSB fraction and higher OA concentrations preserve a greater presence of functional groups (Lonappan et al., 2020), increasing chemical reactivity, although with lower structural stability of C. Similar increases in oxygen-containing functional groups after chemical or acidic activation have been reported for modified biochars, indicating enhanced surface functionalization and reactivity (Murtaza et al., 2024).

Compared to SS, BBFs tend to exhibit characteristics indicative of a higher degree of C structural stabilization. Fertilizers produced with SSB500, whether without OA or with a low concentration of this acid, tend to favor C stabilization more strongly. In contrast, fertilizers formulated from SSB300 have a lower capacity to promote this stabilization.

3.2.2.2. Oxidative resistance indicators. The VM/FC ratio varied significantly between treatments ($p < 0.05$) (Fig. 7A), reflecting differences in the relative distribution between labile and recalcitrant C fractions in SS biochars. The VM/FC ratio provides a more accurate assessment of biochar stability (Leng et al., 2019). Higher VM/FC values indicate a greater proportion of volatile compounds and therefore lower relative resistance to oxidation, while lower values are associated with higher FC

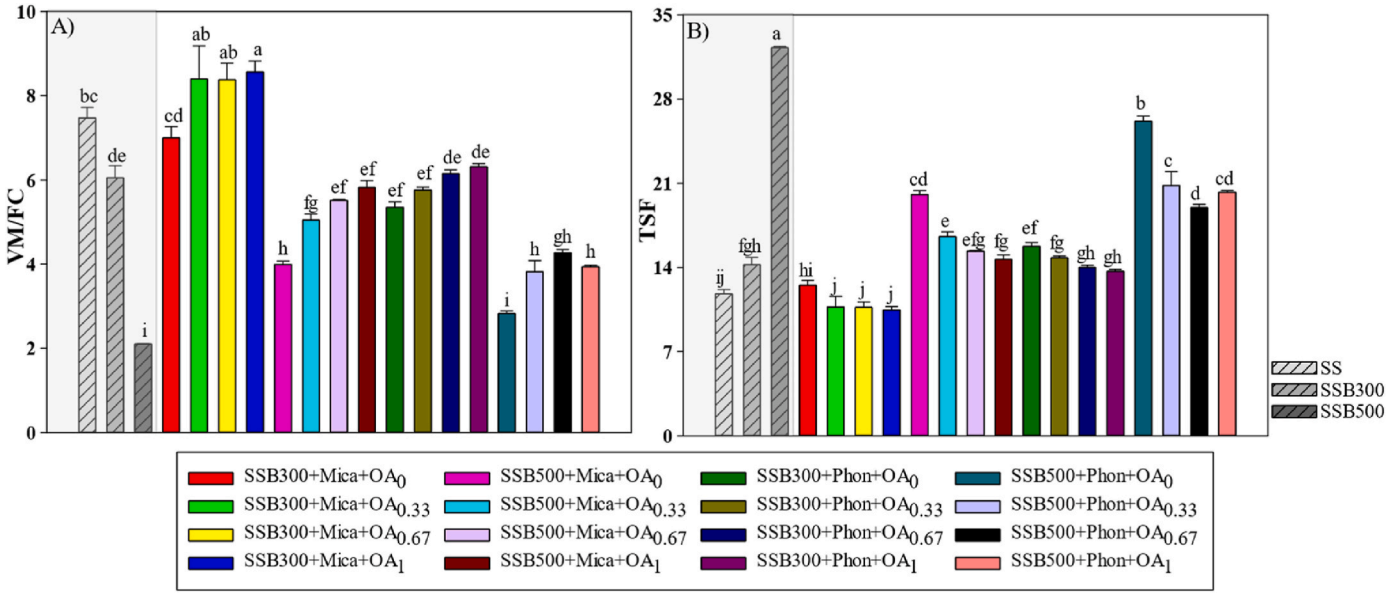

Fig. 7. (A) Volatile matter to fixed C ratio (VM/FC) and (B) Thermostable fraction (TSF) of sewage sludge biochar-based fertilizers (SSB), mica schist (Mica) and phonolite (Phon) subjected to different concentrations of oxalic acid (OA). Different letters indicate significant differences among treatments according to Tukey's test ($p < 0.05$).

content and greater structural stability (Wang et al., 2022). Overall, fertilizers produced with SSB300 had higher VM/FC values than those produced with SSB500 ($P < 0.05$), indicating a greater presence of thermally less-stable organic fractions. In fertilizers containing Mica, the VM/FC values of fertilizers produced with SSB300 ranged from 7.0 to 8.6, while fertilizers produced with SSB500 showed significantly lower values, between 4.0 and 5.8. A similar trend was observed in the Phon treatments, with even lower VM/FC values in the SSB500 formulations. This behavior may be associated with the lower proportion of the mineral fraction in formulations with Phon, which exhibited a higher relative content of SSB. Thus, the lower dilution of pyrolytic C by inorganic components contributes to reduced VM/FC values, reflecting a higher degree of carbonization of the material. Furthermore, these results confirm that increasing the pyrolysis temperature promotes the conversion of volatile C into FC, reducing the labile fraction and increasing the recalcitrance of the material (Zhang et al., 2026). Thus, lower VM/FC values in fertilizers with SSB500 indicate a higher degree of carbonization and thermal maturity of C, reflecting more condensed structures and potentially lower susceptibility to chemical and biological transformations (D'Ávila et al., 2025; Min et al., 2022).

The OA exerted a consistent effect on the volatile mineral content (VM/FC) ratio, particularly in fertilizers produced with SSB300. The progressive increase in acid concentration from 0 mol L^{-1} to 0.33 mol L^{-1}, 0.67 mol L^{-1}, and 1 mol L^{-1} resulted in increases in VM/FC values, indicating a greater presence of volatile fractions. However, in fertilizers produced with SSB500, especially those with Phon, increasing the OA concentration from 0.33 mol L^{-1} to 1 mol L^{-1} did not result in significant increases in VM/FC, suggesting that in more carbonized materials, the condensed aromatic matrix, present in a higher proportion, is less sensitive to acid attack, maintaining a high proportion of FC.

The TSF values varied significantly among the BBFs ($p < 0.05$) (Fig. 7B). The results highlight the combined influence of biochar pyrolysis temperature, the relative biochar-to-agromineral ratio, and OA concentration. In general, fertilizers produced with SSB500 showed higher TSF values than those obtained with SSB300, regardless of the ASi used. As mentioned earlier, this behavior is associated with a higher degree of aromatization and structural condensation in biochar produced at higher temperatures, resulting in higher apparent recalcitrance of organic matter and greater resistance to thermal degradation (Yuan et al., 2015). The addition of OA promoted a progressive reduction in TSF, with a more pronounced effect at higher concentrations (0.67 mol L^{-1} and 1 mol L^{-1}). Acid treatment induces partial solubilization of mineral components and modifies organomineral interactions (Santos et al., 2026). Additionally, OA-induced surface oxidation of biochar can increase the proportion of oxygenated functional groups, thereby raising the thermolabile fraction at the expense of the thermostable fraction, as observed in the FTIR analysis (Fig. 5). This effect was particularly evident in fertilizers formulated with Phon and SSB500, in which the initial TSF was higher due to the greater amount of SSBs in the formulation and was therefore more sensitive to the acid treatment. Even with the application of OA, fertilizers containing SSB500 maintained higher TSF values than those in treatments with SSB300, indicating that pyrolysis temperature plays a dominant role in determining fertilizer thermal stability.

The R_{50} index is widely used as an indicator of the thermal stability of organic matter, as it is directly related to the degree of aromaticity and the recalcitrance of the C present. In fertilizers formulated with SSB300, regardless of the agromineral used (Mica or Phon), the R_{50} values were not highly sensitive to increases in OA concentration (Fig. S5A–B). Despite this, fertilizers produced with SSB500 showed higher R_{50} values in the absence of OA, in both formulations with Mica and Phon (Fig. S5C–D). The addition of OA led to a gradual reduction in R_{50} values, particularly in fertilizers with SSB500, an effect observed consistently in both Mica and Phon. This result suggests that acid treatment, especially at higher concentrations (0.67 mol L^{-1} and 1 mol L^{-1}), can alter the biochar structure and organomineral interactions, promoting surface oxidation and increasing the proportion of functional groups more susceptible to thermal degradation. Consequently, the temperature required to achieve 50% mass loss is reduced. For control purposes, the R_{50} values of SS, SSB300, and SSB500 are presented in Fig. S6, which shows an increase in R_{50} with increasing pyrolysis temperature.

3.2.3. Indicators associated with potential for C sequestration

The temperatures related to C sequestration potential presented in this study are based on indirect indicators of C stability and recalcitrance, including elemental ratios, thermal indices, and spectroscopic characteristics, rather than direct measurements of long-term C persistence in soil.

The C sequestration potential of BBFs was evaluated using indirect indicators based on the relationship among FC, VM and ash content, as shown in the ternary diagram (Fig. 8). This approach allows the classification of materials according to their potential to stabilize C in the soil and is widely used to differentiate materials with high, moderate, or low C sequestration potential (Adhikari et al., 2024; Costa et al., 2025; Enders et al., 2012). Biochars with VM > 80% show no C sequestration potential, while VM < 80% show moderate to high C sequestration potential, which is differentiated by FC concentration and ash content (Adhikari et al., 2024; Enders et al., 2012). Biochar with FC > 60% and ash content <40% increases the C sequestration potential (Adhikari et al., 2024).

In general, all the fertilizers evaluated were concentrated in the lower region of the diagram, characterized by high ash content and low FC fraction, and predominantly positioned in the region classified as having moderate C sequestration potential. This behavior reflects the organomineral nature of the materials, in which the high proportion of ASi (Mica or Phon) probably results in dilution of the structurally stable C content present in the SSB. However, a clear influence of biochar pyrolysis temperature on fertilizer distribution was evident in the diagram. Fertilizers formulated with SSB500 showed a relative shift towards higher FC and lower VM than those formulated with SSB300. This behavior suggests characteristics consistent with a higher degree of aromaticity and greater resistance to degradation, characteristics associated with greater long-term C sequestration potential (Adhikari et al., 2024). The influence of the ASi type was also evident. In general, fertilizers formulated with Phon showed a slight shift towards higher FC content than those formulated with Mica, especially in the SSB500 treatments. This result is attributed to the lower proportion of rock used in the Phon formulation, leading to a higher relative contribution of SSB in the final material. The addition of OA promoted subtle changes in the position of the points on the ternary diagram, without substantially modifying the classification of the C sequestration potential. At higher concentrations (0.67 mol L^{-1} and 1 mol L^{-1}), a slight increase in VM and a reduction in FC were observed, indicating that acid treatment can promote functionalization and partial oxidation of biochar, reducing its structural recalcitrance and, consequently, its C sequestration potential (Xie et al., 2023).

Although none of the fertilizers were positioned in the high C sequestration potential region, the results indicate that the BBFs have moderate potential, remaining in the SS, SSB300, and SSB500 ranges. Compared to other organomineral fertilizers, this represents a significant environmental gain. In general, organomineral fertilizers without biochar exhibit lower C stability and persistence in the soil (Xie et al., 2023). Thus, the data suggest that, although the evaluated BBFs are not primarily intended for C sequestration, the choice of biochar with a higher pyrolysis temperature, combined with formulations with a higher relative proportion of C and lower intensity of acid treatment, can significantly increase the potential for C stabilization in the soil, adding environmental value to the developed fertilizers. Furthermore, the results of this study indicate that biochars derived from other C-rich raw materials can be used to synthesize BBFs with high C sequestration

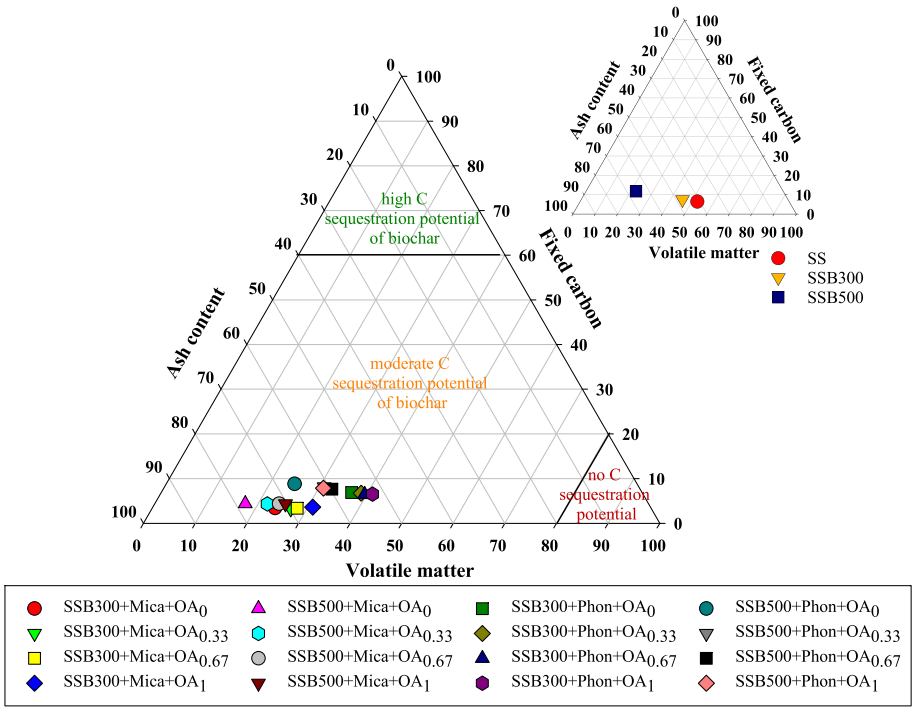

Fig. 8. Ternary diagram of fertilizers based on sewage sludge biochar (SSB), mica schist (Mica) and phonolite (Phon) subjected to different concentrations of oxalic acid (OA).

potential.

The indirect indicator of C sequestration potential estimated using on equation (7), which considers the final amount of C that would remain retained in the soil, subtracting the C lost during the initial pyrolysis in the raw biomass and multiplying by the C recalcitrance (R_{50}), was affected by the biochar pyrolysis temperature, the proportion of added agromineral, and the concentration of active organic matter ($p < 0.05$) (Fig. 9). Fertilizers produced with SSB300 showed a higher C sequestration potential than those produced with SSB500, especially when combined with Phon. This behavior is associated with the higher concentration of C present in SSB300 after pyrolysis (Table S1) combined with the SSB:agromineral ratio present in the formulation. A progressive reduction in C sequestration potential was observed as acid concentration increased, particularly in fertilizers with SSB500. This indicates that high concentrations of OA can intensify mineral dissolution and mobilization of soluble C, reducing its stabilization in the system. Thus, the results suggest that the combination of SSB300 and Phon, regardless of OA concentration, was the most effective at maximizing C sequestration potential. Conversely, the use of SSB500 with Phon in the presence of OA reduced C sequestration potential. Compared with SSBs, there is a reduction in C sequestration potential, due to the biochar/ASi ratio used in formulating the new fertilizers. These findings suggest that the pyrolysis temperature, the intensity of chemical activation, and the type and proportion of agromineral act in an integrated manner to determine the C stabilization of BBFs.

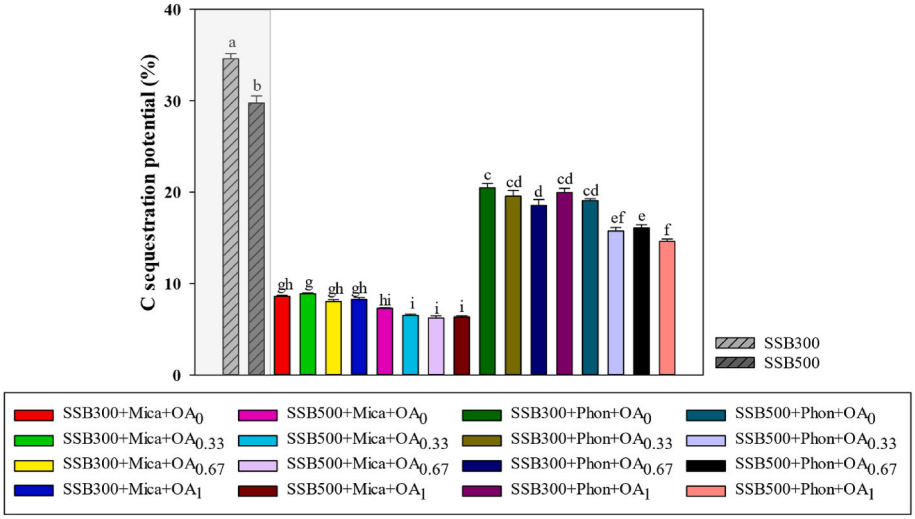

Fig. 9. Potential for C sequestration of sewage sludge biochar-based fertilizers (SSB), mica schist (Mica) and phonolite (Phon) subjected to different concentrations of oxalic acid (OA). Different letters indicate significant differences among treatments according to Tukey's test ($p < 0.05$).

3.3. Principal component analysis

The first two components (PC1 and PC2) of the principal component analysis (PCA) explained 69.49% of the total variance of the BBF properties (Fig. 10). The component matrix is presented in Table S5. Based on the combined analysis of chemical, physical, mineralogical, and C-stability characteristics, the fertilizers were separated into 4 groups: SSB300+Mica, SSB500+Mica, SSB300+Phon, and SSB500+Phon. Therefore, in general, the characteristics of the BBFs are influenced by the pyrolysis temperature and the type of agromineral. It is observed that the small influence of the OA is more evident in the BBFs with biochar produced at 500 °C.

PC1 explains a distinction between the organic fraction derived from SSBs and the mineral fraction from ASi. Positive PC1 values are associated with formulations with a greater contribution from SSB, reflected by higher C and P contents, while negative values indicate a greater influence of the mineral fraction, especially associated with minerals rich in K and Fe. Thus, PC1 can be interpreted as a structural axis of organomineral differentiation, separating formulations dominated by SSB from those with a greater participation of ASi.

PC2 clearly indicates the distinction of BBFs according to the stability and structure of C and was consistent with the trends observed in the Van Krevelen diagram, the VM/FC ratio, and the R_{50} index. Positive values are associated with materials with higher H/C ratios, higher VM/FC ratios, and higher content of oxygenated groups, typical characteristics of less aromatic and more labile structures (P P. Zhang et al., 2022), coinciding with the formulations obtained with SSB300. The values increased with increasing OA concentration, especially in the presence of mica schist, where the SSB/ASi ratio is lower. In contrast, negative values are related to higher R_{50} and TSF values, indicators widely used to estimate the recalcitrance and thermal resistance of C (Leng et al., 2019), coinciding with the formulations prepared with SSB500. Thus, PC2 distinguishes formulations with more functionalized and reactive C from those with a higher degree of aromaticity and oxidative stability, with this behavior being strongly influenced by the pyrolysis temperature of the biochar. The convergence between the PCA, the Van Krevelen diagram, and the thermal stability indices suggests that the pyrolysis temperature was the main controlling factor of the structural organization and C persistence in the BBFs. Although the effect of pyrolysis temperature was predominant, a slight influence of OA addition was observed within the groups, suggesting that chemical activation increased surface functionalization and C reactivity.

Thus, the integrated analysis suggests that the pyrolysis temperature was the primary determinant of the C structural stability (PC2), whereas the proportion and type of agromineral exerted a greater influence on the compositional and nutritional differentiation of the fertilizers (PC1). This partial dissociation between C stability and mineral composition indicates that structural and nutritional attributes can be independently modulated by adjusting production conditions and organomineral proportions. In practical terms, formulations based on SSB500 tend to exhibit greater recalcitrance and persistence in soil, while those derived from SSB300, especially in the presence of OA, exhibit a higher density of functional groups and greater chemical reactivity. Thus, the PCA suggests that the developed BBFs may exhibit multifunctional behavior, in which C stability and nutritional contribution can be strategically balanced according to the intended agronomic and/or environmental objective.

From an agronomic perspective, BBFs produced with SSB500 tend to be more stable, with higher aromaticity and carbon recalcitrance, making them better suited for long-term strategies to increase carbon persistence in soil. These characteristics are desirable in systems focused on improving soil quality and mitigating emissions, although they may offer lower immediate nutrient availability than conventional soluble fertilizers. In contrast, materials produced at 300 °C have a higher proportion of labile structures and reactive functional groups, particularly in the presence of OA, leading to greater interaction with the mineral fraction and a higher density of active sites. This enhances nutrient availability, bringing their behavior closer to that of conventional fertilizers. Therefore, the selection of the most appropriate formulation depends on the producer's specific management goals.

Compared to conventional fertilizers, the developed materials offer significant advantages, including stable carbon content and a multifunctional design that integrates chemical, physical, and mineralogical attributes within a single matrix. These characteristics are particularly relevant given that the production and use of conventional fertilizers account for approximately 15% of agricultural greenhouse gas emissions (Bolan et al., 2026), reinforcing the importance of developing alternative fertilization strategies based on waste valorization and C stabilization. Furthermore, the association between biochar and agrominerals promotes the formation of complex organomineral systems with greater potential for soil interactions. On the other hand, their main limitations include greater compositional heterogeneity, dependence on production conditions, such as temperature and chemical activation, in defining the final properties; and lower standardization compared to conventional

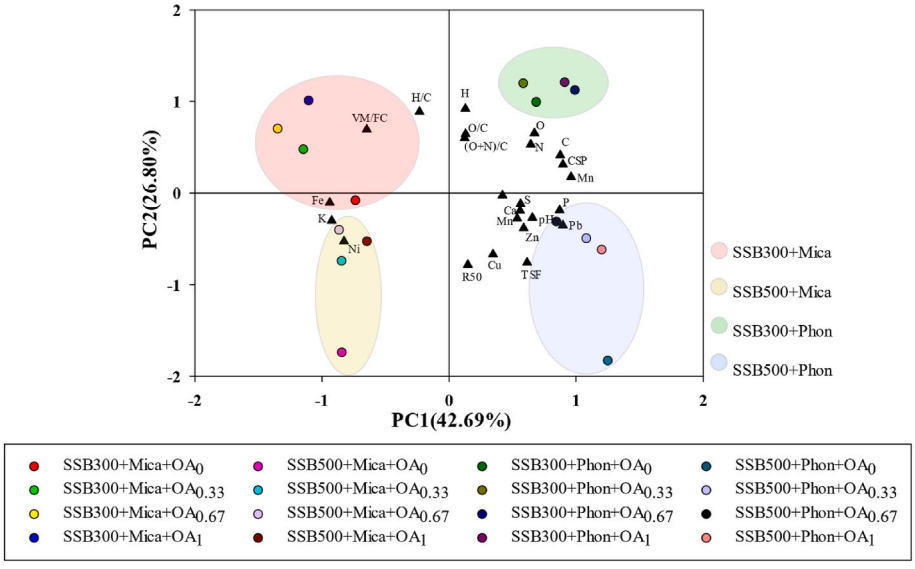

Fig. 10. Principal component analysis of sewage sludge biochar-based fertilizers (SSB), mica schist (Mica) and phonolite (Phon) subjected to different concentrations of oxalic acid (OA).

fertilizers, which may hinder their direct agronomic recommendation.

4. Conclusions

Sewage sludge biochar-based fertilizers enriched with silicate agrominerals (ASi) and oxalic acid (OA) exhibited chemical, structural, and thermal properties that were significantly influenced by pyrolysis temperature and the proportion of agromineral added. The use of SSB500 in the formulation promoted greater aromaticity and oxidative stability of C, indicating properties associated with greater resistance to thermal degradation and characteristics consistent with greater persistence in soil. In contrast, formulations using SSB300 showed a higher density of functional groups and greater structural reactivity, characteristics that may favor the retention, exchange, and gradual availability of nutrients in the soil. Thus, there is no single optimal temperature, but rather a functional trade-off: higher temperatures (500 °C) tend to promote greater C stability, whereas lower temperatures (300 °C) favor functionalization and reactivity, making the choice dependent on the agronomic objective of the formulation. Therefore, if the primary focus is enhanced chemical reactivity and potential nutrient release, formulations based on SSB300 should be prioritized. The incorporation of Mica and Phon increased the total levels of K and other mineral elements, with a clear compositional difference observed between the organic and mineral fractions through multivariate analysis. The application of OA promoted structural changes in the mineral matrix and in the C structure, with a slight reduction in recalcitrance and a possible increase in nutrient availability. In general, the developed materials show potential as multifunctional organomineral fertilizers, integrating residue valorization, nutrient-release potential, and a moderate contribution to soil C stabilization, from a sustainability and circular economy perspective.

However, no single BBF formulation emerged as ideal across the evaluated combinations. Variations in pyrolysis temperature, agromineral type, and oxalic acid concentration yield materials with distinct and, to some extent, complementary properties. This lack of a single optimal formulation reflects the multifunctional nature of these fertilizers, in which attributes such as carbon stability, surface reactivity, and mineral composition can be tailored to the intended application. Therefore, selecting the most appropriate formulation should consider the specific agronomic context, soil characteristics, and management goals, rather than seeking a single standard of performance. This flexibility is a key advantage over conventional fertilizers, enabling the design of customized formulations for different soil conditions and crops. Further studies should focus on evaluating the dynamics of nutrient release in soil and conducting agronomic trials in greenhouses and fields to validate the formulations' performance under real-world conditions. Studies on the mobility and ecotoxicity of toxic metals are also necessary, ensuring long-term environmental safety. In parallel, the optimization of organomineral proportions, the economic feasibility analysis, and the life cycle assessment of the process are essential steps to enable industrial-scale application. The integration of these approaches may support the consolidation of these fertilizers as a sustainable alternative in agricultural systems aligned with the principles of the circular economy.

CRediT authorship contribution statement

Marcela Granato Barbosa dos Santos: Conceptualization, Formal analysis, Writing – original draft, Writing – review & editing. **José Ferreira Lustosa Filho:** Writing – original draft, Writing – review & editing. **Camila Rodrigues Costa:** Formal analysis, Methodology. **Beatriz Carvalho Lima:** Formal analysis, Methodology. **Maíra Lopes D'Ávila:** Formal analysis, Methodology. **Sérgio Sirilo de Oliveira:** Formal analysis, Methodology. **Gilberto de Oliveira Mendes:** Conceptualization, Writing – review & editing. **Éder de Souza Martins:** Conceptualization, Writing – review & editing. **Giuliano Marchi:** Writing – review & editing. **Cícero Célio de Figueiredo:** Conceptualization, Supervision, Writing – review & editing.

Declaration of competing interest

The authors declare that they have no known competing financial interests or personal relationships that could have appeared to influence the work reported in this paper.

Acknowledgements

We acknowledge the Conselho Nacional de Desenvolvimento Científico e Tecnológico (CNPq) for the scientific productivity fellowship granted to Cícero Célio de Figueiredo (Grant number 305176/2023-4) and Gilberto de Oliveira Mendes (Grant number 314216/2023-5). The authors thank the Coordenação de Aperfeiçoamento de Pessoal de Nível Superior (CAPES), the Fundação de Apoio à Pesquisa do Distrito Federal (grant number 00193-00002230/2022-71), and Fundação de Amparo à Pesquisa do Estado de Minas Gerais (grant number APQ-02351-23) for the financial support provided for the realization of this study.

Appendix A. Supplementary data

Supplementary data to this article can be found online at https://doi.org/10.1016/j.jenvman.2026.130107.

Data availability

Data will be made available on request.

References

Adhikari, S., Moon, E., Paz-Ferreiro, J., Timms, W., 2024. Comparative analysis of biochar carbon stability methods and implications for carbon credits. Sci. Total Environ. 914, 169607. https://doi.org/10.1016/j.scitotenv.2023.169607.

Aktar, S., Hossain, M.A., Rathnayake, N., Patel, S., Gasco, G., Mendez, A., de Figueiredo, C., Surapaneni, A., Shah, K., Paz-Ferreiro, J., 2022. Effects of temperature and carrier gas on physico-chemical properties of biochar derived from biosolids. J. Anal. Appl. Pyrolysis 164, 105542. https://doi.org/10.1016/j.jaap.2022.105542.

American Society for Testing and Materials, 2013. ASTM D1762: Standard Test Method for Chemical Analysis of Wood Charcoal. West Conshohocken, PA.

Antunes, E., Schumann, J., Brodie, G., Jacob, M.V., Schneider, P.A., 2017. Biochar produced from biosolids using a single-mode microwave: characterisation and its potential for phosphorus removal. J. Environ. Manag. 196, 119–126. https://doi.org/10.1016/j.jenvman.2017.02.080.

Awoniyi, A.S., Adeyemo, A.J., Agbenin, J.O., Ilori, A.O., da Silva Oliveira, D.M., de Freitas, D.A.F., 2025. Potassium release from K-bearing minerals treated with organic acids under laboratory conditions. Discover Soil 2, 69. https://doi.org/10.1007/s44378-025-00096-7.

Boehm, S., Jeffery, L., Hecke, J., Schumer, C., Jaeger, J., Fyson, C., Levin, K., Nilsson, A., Naimoli, S., Daly, E., Thwaites, J., Lebling, K., Waite, R., Collis, J., Sims, M., Singh, N., Grier, E., Lamb, W., Castellanos, S., Lee, A., Geffray, M.-C., Santo, R., Balehegn, M., Petroni, M., Masterson, M., 2023. State of Climate Action 2023. World Resources Institute. https://doi.org/10.46830/wrirpt.23.00010.

Bolan, N., Lv, X., Xu, Y., Mondal, T., Bolan, S., Smith, P., Campbell, G.A., Mukherjee, S., Kelbel, G., Chadalavada, S., Siddique, K.H.M., 2026. Fertiliser use and carbon sequestration in agricultural soils. Agric. Ecosyst. Environ. 407, 110462. https://doi.org/10.1016/j.agee.2026.110462.

Brasil, 2006. Instrução Normativa SDA Nº 27, De 5 De Junho De 2006. Brasília.

Brasil, 2017. Manual De Métodos Analíticos Oficiais Para Fertilizantes E Corretivos. Brasília.

Button, E.S., Pett-Ridge, J., Murphy, D.V., Kuzyakov, Y., Chadwick, D.R., Jones, D.L., 2022. Deep-C storage: biological, chemical and physical strategies to enhance carbon stocks in agricultural subsoils. Soil Biol. Biochem. 170, 108697. https://doi.org/10.1016/j.soilbio.2022.108697.

Cely, P., Gascó, G., Paz-Ferreiro, J., Méndez, A., 2015. Agronomic properties of biochars from different manure wastes. J. Anal. Appl. Pyrolysis 111, 173–182. https://doi.org/10.1016/j.jaap.2014.11.014.

Chagas, J.K.M., de Figueiredo, C.C., Paz-Ferreiro, J., 2021. Sewage sludge biochars effects on corn response and nutrition and on soil properties in a 5-yr field experiment. Geoderma 401, 115323. https://doi.org/10.1016/j.geoderma.2021.115323.

Costa, C.R., de Souza, A.M., dos Santos, M.G.B., da Silva, I.G.R., Moraes, T.V., dos Santos, J.R., de Siqueira Dantas, V.F., Figueiredo, C.C. de, 2025. Stability and carbon sequestration potential of bamboo biochar. Biomass Convers. Biorefin. https://doi.org/10.1007/s13399-025-06632-3.

Cui, X., Li, X., Wang, J., Wang, X., Yu, F., Yang, G., Xu, S., Cheng, Z., Yang, Q., Yan, B., Guanyi, C., 2025. A review on the production of nutrient-enriched biochar: insights from the evolution of nitrogen, phosphorus, and potassium. Crit. Rev. Environ. Sci. Technol. 1–19. https://doi.org/10.1080/10643389.2025.2457991, 0.

Dabare, S., Munaweera, I., 2026. Mechanistic and kinetic insights into organic acid-mediated rock phosphate solubilization for sustainable phosphorus mobilization. J. Soils Sediments 26, 91. https://doi.org/10.1007/s11368-026-04274-0.

Dalton, D.A., Russel, S.A., Evans, H.J., 1988. Nickel as a micronutrient element for plants. Biofactors 1, 11–16.

Duarte, L.M., Xavier, L.V., Rossati, K.F., de Oliveira, V.A., Schimicoscki, R.S., de Ávila Neto, C.N., Mendes, G. de O., 2022. Potassium extraction from the silicate rock verdete using organic acids. Sci. Agric. 79. https://doi.org/10.1590/1678-992x-2020-0164.

D'Ávila, M.L., Lustosa Filho, J.F., Martins, É. de S., Marchi, G., Trindade, G., Costa, C.R., Santos, M.G.B. dos, Sandri, D., Figueiredo, C.C. de, 2025. Co-Pyrolysis of sewage sludge and zeolitic basalt: physicochemical characterization, stability and carbon sequestration potential. Sustainability 18, 258. https://doi.org/10.3390/su18010258.

Enders, A., Hanley, K., Whitman, T., Joseph, S., Lehmann, J., 2012. Characterization of biochars to evaluate recalcitrance and agronomic performance. Bioresour. Technol. 114, 644–653. https://doi.org/10.1016/j.biortech.2012.03.022.

Environmental Protection Agency (USEPA), 1996. Method 3050B - Acid Digestion of Sediments, Sludges, and Soils.

Fachini, J., de Figueiredo, C.C., do Vale, A.T., 2022. Assessing potassium release in natural silica sand from novel K-enriched sewage sludge biochar fertilizers. J. Environ. Manag. 314, 115080. https://doi.org/10.1016/j.jenvman.2022.115080.

Fachini, J., de Figueiredo, C.C., Frazão, J.J., Rosa, S.D., da Silva, J., do Vale, A.T., 2021. Novel K-enriched organomineral fertilizer from sewage sludge-biochar: Chemical, physical and mineralogical characterization. Waste Manag. 135, 98–108. https://doi.org/10.1016/j.wasman.2021.08.027.

Fachini, J., Figueiredo, C.C. de, do Vale, A.T., da Silva, J., Zandonadi, D.B., 2024. Potassium-enriched biochar-based fertilizers for improved uptake in radish plants. Nutr. Cycl. Agroecosyst. 128, 415–427. https://doi.org/10.1007/s10705-023-10273-1.

Fei, H., Hu, D., Zheng, K., Zhang, B., Wang, C., Han, R., 2025. Carbon retention and stability of Ca(OH)2-modified biochar and its impact on carbon sequestration potential in acidic red soil. J. Anal. Appl. Pyrolysis 186, 106961. https://doi.org/10.1016/j.jaap.2025.106961.

Figueiredo, C., Lopes, H., Coser, T., Vale, A., Busato, J., Aguiar, N., Novotny, E., Canellas, L., 2018. Influence of pyrolysis temperature on chemical and physical properties of biochar from sewage sludge. Arch. Agron Soil Sci. 64, 881–889. https://doi.org/10.1080/03650340.2017.1407870.

Figueiredo, C.C., de Souza Prado Junqueira Reis, A., de Araujo, A.S., Blum, L.E.B., Shah, K., Paz-Ferreiro, J., 2021. Assessing the potential of sewage sludge-derived biochar as a novel phosphorus fertilizer: influence of extractant solutions and pyrolysis temperatures. Waste Manag. 124, 144–153. https://doi.org/10.1016/j.wasman.2021.01.044.

Gebretsadkan, A.A., Belete, Y.Z., Krounbi, L., Gelfand, I., Bernstein, R., Gross, A., 2024. Soil application of activated hydrochar derived from sewage sludge enhances plant growth and reduces nitrogen loss. Sci. Total Environ. 949, 174965. https://doi.org/10.1016/j.scitotenv.2024.174965.

Halalsheh, M., Shatanawi, K., Shawabkeh, R., Kassab, G., Mohammad, H., Adawi, M., Ababneh, S., Abdullah, A., Ghantous, N., Balah, N., Almomani, S., 2024. Impact of temperature and residence time on sewage sludge pyrolysis for combined carbon sequestration and energy production. Heliyon 10, e10845. https://doi.org/10.1016/j.heliyon.2024.e28030.

Harvey, O.R., Kuo, L.-J., Zimmerman, A.R., Louchouarn, P., Amonette, J.E., Herbert, B. E., 2012. An index-based approach to assessing recalcitrance and soil carbon sequestration potential of engineered black carbons (biochars). Environ. Sci. Technol. 46, 1415–1421. https://doi.org/10.1021/es2040398.

Hoang, S.A., Bolan, N., Madhubashani, A.M.P., Vithanage, M., Perera, V., Wijesekara, H., Wang, H., Srivastava, P., Kirkham, M.B., Mickan, B.S., Rinklebe, J., Siddique, K.H. M., 2022. Treatment processes to eliminate potential environmental hazards and restore agronomic value of sewage sludge: a review. Environ. Pollut. 293, 118564. https://doi.org/10.1016/j.envpol.2021.118564.

Řimnáčová, D., Bičáková, O., Moško, J., Straka, P., Čimová, N., 2024. The effect of carbonization temperature on textural properties of sewage sludge-derived biochars as potential adsorbents. J. Environ. Manag. 359, 120947. https://doi.org/10.1016/j.jenvman.2024.120947.

Jones, D.L., Cooledge, E.C., Alston, D., Chadwick, D.R., 2026. Agricultural management strategies to actively promote subsoil carbon storage. Soil Tillage Res. 256, 106846. https://doi.org/10.1016/j.still.2025.106846.

Kabata-Pendias, A., 2000. Trace Elements in Soils and Plants. CRC Press. https://doi.org/10.1201/9781420039900.

Kacprzak, M., Baran, J., Fijalkowski, K., 2025. Emerging sewage sludge treatment technologies for land carbon sequestration: a comprehensive review. J. Mater. Cycles Waste Manag. 27, 2866–2886. https://doi.org/10.1007/s10163-025-02369-3.

Kanteraki, A.E., Isari, E.A., Svarnas, P., Kalavrouziotis, I.K., 2022. Biosolids: the trojan horse or the beautiful helen for soil fertilization? Sci. Total Environ. 839, 156270. https://doi.org/10.1016/j.scitotenv.2022.156270.

Keiluweit, M., Nico, P.S., Johnson, M.G., Kleber, M., 2010. Dynamic molecular structure of plant biomass-derived black carbon (biochar). Environ. Sci. Technol. 44, 1247–1253. https://doi.org/10.1021/es9031419.

Kominko, H., Gorazda, K., Wzorek, Z., 2024. Sewage sludge: a review of its risks and circular raw material potential. J. Water Proc. Eng. 63, 105522. https://doi.org/10.1016/j.jwpe.2024.105522.

Košnář, Z., Mercl, F., Pierdonà, L., Chane, A.D., Míchal, P., Tlustoš, P., 2023. Concentration of the main persistent organic pollutants in sewage sludge in relation to wastewater treatment plant parameters and sludge stabilisation. Environ. Pollut. 333, 122060. https://doi.org/10.1016/j.envpol.2023.122060.

Krahl, L.L., Marchi, G., Paz, S.P.A., Angélica, R.S., Sousa-Silva, J.C., Valadares, L.F., Martins, É. de S., 2022a. Increase in cation exchange capacity by the action of maize rhizosphere on Mg or Fe biotite-rich rocks1. Pesqui. Agropecuária Trop. 52. https://doi.org/10.1590/1983-40632022v5272376.

Krahl, L.L., Valadares, L.F., Sousa-Silva, J.C., Marchi, G., de Souza Martins, É., 2022b. Dissolution of silicate minerals and nutrient availability for corn grown successively. Pesqui. Agropecu. Bras. 57. https://doi.org/10.1590/S1678-3921.PAB2022.V57.01467.

Lehmann, J., Joseph, S., 2024. Biochar for Environmental Management. Routledge, London. https://doi.org/10.4324/9781003297673.

Leng, L., Huang, H., Li, H., Li, J., Zhou, W., 2019. Biochar stability assessment methods: a review. Sci. Total Environ. 647, 210–222. https://doi.org/10.1016/j.scitotenv.2018.07.402.

Li, L., Li, H., Tong, L., Lv, Y., 2024. Sustainable agriculture practices: utilizing composted sludge fertilizer for improved crop yield and soil health. Agronomy 14. https://doi.org/10.3390/agronomy14040756.

Li, M., Tang, Y., Ren, N., Zhang, Z., Cao, Y., 2018. Effect of mineral constituents on temperature-dependent structural characterization of carbon fractions in sewage sludge-derived biochar. J. Clean. Prod. 172, 3342–3350. https://doi.org/10.1016/j.jclepro.2017.11.090.

Li, S., Chen, G., 2018. Thermogravimetric, thermochemical, and infrared spectral characterization of feedstocks and biochar derived at different pyrolysis temperatures. Waste Manag. 78, 198–207. https://doi.org/10.1016/j.wasman.2018.05.048.

Liu, G., Chen, L., Jiang, Z., Zheng, H., Dai, Y., Luo, X., Wang, Z., 2017. Aging impacts of low molecular weight organic acids (LMWOAs) on furfural production residue-derived biochars: porosity, functional properties, and inorganic minerals. Sci. Total Environ. 607–608, 1428–1436. https://doi.org/10.1016/j.scitotenv.2017.07.046.

Liu, S., Xie, Z., Zhu, Yintao, Zhu, Yanmiao, Jiang, Y., Wang, Y., Gao, H., 2021. Adsorption characteristics of modified rice straw biochar for Zn and in-situ remediation of Zn contaminated soil. Environ. Technol. Innov. 22, 101388. https://doi.org/10.1016/j.eti.2021.101388.

Lodi, L.A., Klaic, R., Bortoletto-Santos, R., Ribeiro, C., Farinas, C.S., 2022. Unveiling the solubilization of potassium mineral rocks in organic acids for application as K-Fertilizer. Appl. Biochem. Biotechnol. 194, 2431–2447. https://doi.org/10.1007/s12010-022-03826-7.

Lonappan, L., Liu, Y., Rouissi, T., Brar, S.K., Surampalli, R.Y., 2020. Development of biochar-based green functional materials using organic acids for environmental applications. J. Clean. Prod. 244, 118841. https://doi.org/10.1016/j.jclepro.2019.118841.

Lustosa Filho, J.F., da Silva Rodrigues Viana, R., Melo, L.C.A., de Figueiredo, C.C., 2025. Changes in phosphorus due to pyrolysis and in the soil-plant system amended with sewage sludge biochar compared to conventional P fertilizers: a global meta-analysis. Chemosphere 371, 144055. https://doi.org/10.1016/j.chemosphere.2024.144055.

Lustosa Filho, J.F., Lima, B.C., Costa, J. da L., Santos, M.G.B. dos, Costa, C.R., Oliveira, S. S. de, Mendes, G. de O., Fachini, J., Figueiredo, C.C. de, 2026. Oxalic acid enhances the performance of potassium-enriched biochar-based fertilizers. Biomass Bioenergy 208, 108912. https://doi.org/10.1016/j.biombioe.2025.108912.

Makowska, D., Pandiyan, M., Kapusta, K., Kolarz, K., Stypka, Z., Boehman, A.L., Wooldridge, M.S., 2025. Effects of pyrolysis parameters on biochar derived from sewage sludge including environmental risk assessment of heavy metals. J. Environ. Manag. 395, 127888. https://doi.org/10.1016/j.jenvman.2025.127888.

Malavolta, E., 2006. Manual De Nutrição Mineral De Plantas. Ceres, Piracicaba.

Martins, É. de S., Rodrigues Júnior, E., Marchi, G., Vilela, G.F., Swoboda, P., Silveira, C. A.P., Martins, E. de S., Hardoim, P., Theodoro, S.H., 2026. Chemical and mineralogical classification of silicate agrominerals. In: de Souza Martins, É., Huff Theodoro, S. (Eds.), Soil Remineralizers and Silicate Fertilizers: Regional Solutions to a Healthy Agriculture. Springer, Nature Switzerland, Cham, pp. 49–68. https://doi.org/10.1007/978-3-032-14656-4_3.

Mbasabire, P., Murindangabo, Y.T., Frouz, J., Brom, J., 2024. Characterization, fractionation and untapped potential of phosphate-amended sewage sludge biochar in soil-plant systems. Chemosphere 367, 143565. https://doi.org/10.1016/j.chemosphere.2024.143565.

Melo, V. de F., Alleoni, L.R.F., 2019. Química E Mineralogia Do Solo: Conceitos Básicos E Aplicações, MG. SBCS, Viçosa.

Mendes, G. de O., Dyer, T., Csetenyi, L., Gadd, G.M., 2022. Rock phosphate solubilization by abiotic and fungal-produced oxalic acid: reaction parameters and bioleaching potential. Microb. Biotechnol. 15, 1189–1202. https://doi.org/10.1111/1751-7915.13792.

Mendes, G. de O., Murta, H.M., Valadares, R.V., da Silveira, W.B., da Silva, I.R., Costa, M. D., 2020. Oxalic acid is more efficient than sulfuric acid for rock phosphate solubilization. Miner. Eng. 155, 106458. https://doi.org/10.1016/j.mineng.2020.106458.

Min, X., Ge, T., Li, Hui, Shi, Y., Fang, T., Sheng, B., Li, Huaiyan, Dong, X., 2022. Combining impregnation and co-pyrolysis to reduce the environmental risk of biochar derived from sewage sludge. Chemosphere 290, 133371. https://doi.org/10.1016/j.chemosphere.2021.133371.

Murtaza, G., Ahmed, Z., Valipour, M., Ali, I., Usman, M., Iqbal, R., Zulfiqar, U., Rizwan, M., Mahmood, S., Ullah, A., Arslan, M., Rehman, M.H. ur, Ditta, A., Tariq, A., 2024. Recent trends and economic significance of modified/functionalized

biochars for remediation of environmental pollutants. Sci. Rep. 14, 217. https://doi.org/10.1038/s41598-023-50623-1.
Ndoung, O.C.N., de Souza, L.R., Fachini, J., Leão, T.P., Sandri, D., de Figueiredo, C.C., 2023. Dynamics of potassium released from sewage sludge biochar fertilizers in soil. J. Environ. Manag. 346, 119057. https://doi.org/10.1016/j.jenvman.2023.119057.
Panahi, H.K.S., Dehhaghi, M., Ok, Y.S., Nizami, A.-S., Khoshnevisan, B., Mussatto, S.I., Aghbashlo, M., Tabatabaei, M., Lam, S.S., 2020. A comprehensive review of engineered biochar: production, characteristics, and environmental applications. J. Clean. Prod. 270, 122462. https://doi.org/10.1016/j.jclepro.2020.122462.
Pariyar, P., Kumari, K., Jain, M.K., Jadhao, P.S., 2020. Evaluation of change in biochar properties derived from different feedstock and pyrolysis temperature for environmental and agricultural application. Sci. Total Environ. 713, 136433. https://doi.org/10.1016/j.scitotenv.2019.136433.
Patel, S., Hakeem, I.G., Marzbali, M.H., Halder, P., Vuppaladadiyam, A.K., Kumar, L., Surapaneni, A., Sharma, A., Batstone, D.J., Shah, K., 2026. Thermal treatment options for biosolids management: a critical review. Environ. Sci. 12, 93–120. https://doi.org/10.1039/D5EW00569H.
Paz-Ferreiro, J., Nieto, A., Méndez, A., Askeland, M.P.J., Gascó, G., 2018. Biochar from biosolids pyrolysis: a review. Int. J. Environ. Res. Publ. Health. https://doi.org/10.3390/ijerph15050956.
Raj, A., Yadav, A., Arya, S., Sirohi, R., Kumar, S., Rawat, A.P., Thakur, R.S., Patel, D.K., Bahadur, L., Pandey, A., 2021. Preparation, characterization and agri applications of biochar produced by pyrolysis of sewage sludge at different temperatures. Sci. Total Environ. 795, 148722. https://doi.org/10.1016/j.scitotenv.2021.148722.
Rehman, M.Z. ur, Batool, Z., Ayub, M.A., Hussaini, K.M., Murtaza, G., Usman, M., Naeem, A., Khalid, H., Rizwan, M., Ali, S., 2020. Effect of acidified biochar on bioaccumulation of cadmium (cd) and rice growth in contaminated soil. Environ. Technol. Innov. 19, 101015. https://doi.org/10.1016/j.eti.2020.101015.
Riemenschneider, W., Tanifuji, M., 2011. Oxalic acid. In: Ullmann's Encyclopedia of Industrial Chemistry. Wiley. https://doi.org/10.1002/14356007.a18_247.pub2.
Rydgård, M., Bairaktari, A., Thelin, G., Bruun, S., 2024. Application of untreated versus pyrolysed sewage sludge in agriculture: a life cycle assessment. J. Clean. Prod. 454, 142249. https://doi.org/10.1016/j.jclepro.2024.142249.
Santos, M.G.B. dos, Costa, C.R., Mendes, G. de O., Paiva, A.B., Peixoto, L.S., Costa, J. da L., Marchi, G., Martins, É. de S., Figueiredo, C.C. de, 2024. Oxalic acid boosts phosphorus release from sewage sludge biochar: a key mechanism for biochar-based fertilizers. Agriculture (Switzerland) 14. https://doi.org/10.3390/agriculture14091607.
Santos, M.G.B. dos, Paiva, A.B., Costa, C.R., Paiva, M.B., Mendes, G. de O., Martins, É. de S., Marchi, G., Lustosa Filho, J.F., Figueiredo, C.C. de, 2026. The role of oxalic acid in nutrient solubilization, potentially toxic elements from sewage sludge biochar, and remineralizers for sustainable local fertilizers. Environ. Res. 294, 123818. https://doi.org/10.1016/j.envres.2026.123818.
Santoyo, G., Mendes, G. de O., Orozco-Mosqueda, Ma del C., Morales-Sandoval, P.H., Parra-Cota, F.I., Santos-Villalobos, S. de los, Li, H., Li, Z., López-Arredondo, D., Herrera-Estrella, L.R., 2026. Phosphorus-solubilizing microorganisms: advances in nutrient uptake mechanisms, plant growth promotion, and sustainable agriculture. Microbiol. Res. 305, 128419. https://doi.org/10.1016/j.micres.2025.128419.
Schreiter, I.J., Schmidt, W., Schüth, C., 2018. Sorption mechanisms of chlorinated hydrocarbons on biochar produced from different feedstocks: conclusions from single- and bi-solute experiments. Chemosphere 203, 34–43. https://doi.org/10.1016/j.chemosphere.2018.03.173.
Sivaranjanee, R., Kumar, P.S., Rangasamy, G., 2023. A critical review on biochar for environmental applications. Carbon Lett. 33, 1407–1432. https://doi.org/10.1007/s42823-023-00527-x.
Skorina, T., Allanore, A., 2015. Aqueous alteration of potassium-bearing aluminosilicate minerals: from mechanism to processing. Green Chem. 17, 2123–2136. https://doi.org/10.1039/C4GC02084G.
Spokas, K.A., 2010. Review of the stability of biochar in soils: predictability of O:C molar ratios. Carbon Manag. 1, 289–303. https://doi.org/10.4155/cmt.10.32.
Tariq, F.S., 2021. Heavy metals concentration in vegetables irrigated with municipal wastewater and their human daily intake in erbil city. Environ. Nanotechnol. Monit. Manag. 16, 100475. https://doi.org/10.1016/j.enmm.2021.100475.
Trani, P.E., Trani, A.L., 2011. Fertilizantes: Cálculo De Fórmulas Comerciais. Campinas.
Van Straaten, Peter, 2007. Agrogeololgy : the Use of Rocks for Crops. Enviroquest Ltd. & Peter van Straaten.
Vause, D., Heaney, N., Lin, C., 2018. Differential release of sewage sludge biochar-borne elements by common low-molecular-weight organic acids. Ecotoxicol. Environ. Saf. 165, 219–223. https://doi.org/10.1016/j.ecoenv.2018.09.005.
Volpi, M.P.C., Silva, J.C.G., Hornung, A., Ouadi, M., 2024. Review of the current state of pyrolysis and biochar utilization in Europe: a scientific perspective. Clean Technologies. https://doi.org/10.3390/cleantechnol6010010.
Wang, L., Olsen, M.N.P., Moni, C., Dieguez-Alonso, A., de la Rosa, J.M., Stenrød, M., Liu, X., Mao, L., 2022. Comparison of properties of biochar produced from different types of lignocellulosic biomass by slow pyrolysis at 600 °C. Applications in Energy and Combustion Science 12, 100090. https://doi.org/10.1016/j.jaecs.2022.100090.
Werle, S., Sobek, S., 2019. Gasification of sewage sludge within a circular economy perspective: a Polish case study. Environ. Sci. Pollut. Control Ser. 26, 35422–35432. https://doi.org/10.1007/s11356-019-05897-2.
Wijesekara, H., Bolan, N.S., Kumarathilaka, P., Geekiyanage, N., Kunhikrishnan, A., Seshadri, B., Saint, C., Surapaneni, A., Vithanage, M., 2016. Chapter 3 - biosolids enhance mine site rehabilitation and revegetation. In: Prasad, M.N.V., Shih, K. (Eds.), Environmental Materials and Waste. Academic Press, pp. 45–71. https://doi.org/10.1016/B978-0-12-803837-6.00003-2.
Xie, S., Tran, H.-T., Pu, M., Zhang, T., 2023. Transformation characteristics of organic matter and phosphorus in composting processes of agricultural organic waste: research trends. Mater. Sci. Energy Technol. 6, 331–342. https://doi.org/10.1016/j.mset.2023.02.006.
Xu, Q., Zhang, F., Song, F., Guo, H., Wang, X., Bi, F., Xu, M., 2024. Investigating CO_2 sequestration via enhanced rock weathering: effects of temperature and citric acid on dolomite and basalt. J. Clean. Prod. 485, 144414. https://doi.org/10.1016/j.jclepro.2024.144414.
Xu, X., Zhao, Y., Sima, J., Zhao, L., Mašek, O., Cao, X., 2017. Indispensable role of biochar-inherent mineral constituents in its environmental applications: a review. Bioresour. Technol. 241, 887–899. https://doi.org/10.1016/j.biortech.2017.06.023.
Yi, B., Guo, F., Wei, Q., Huang, F., Senadheera, S.S., Mašek, O., Sarmah, A.K., Rinklebe, J., Ok, Y.S., 2025. Functionalized biochar: mechanisms of oxygen-containing functional groups in water pollutant remediation. ACS ES&T Water 5, 5764–5784. https://doi.org/10.1021/acsestwater.5c00416.
Yuan, H., Lu, T., Huang, H., Zhao, D., Kobayashi, N., Chen, Y., 2015. Influence of pyrolysis temperature on physical and chemical properties of biochar made from sewage sludge. J. Anal. Appl. Pyrolysis 112, 284–289. https://doi.org/10.1016/j.jaap.2015.01.010.
Zhang, H., Li, Q., Zhang, X., Chen, W., Ni, J., Yang, L., Wei, R., 2020. Insight into the mechanism of low molecular weight organic acids-mediated release of phosphorus and potassium from biochars. Sci. Total Environ. 742, 140416. https://doi.org/10.1016/j.scitotenv.2020.140416.
Zhang, H., Qi, H.-Y., Zhang, Y.-L., Ran, D.-D., Wu, L.-Q., Wang, H.-F., Zeng, R.J., 2022. Effects of sewage sludge pretreatment methods on its use in agricultural applications. J. Hazard. Mater. 428, 128213. https://doi.org/10.1016/j.jhazmat.2022.128213.
Zhang, P., Duan, W., Peng, H., Pan, B., Xing, B., 2022. Functional biochar and its balanced design. ACS Environ. Au 2, 115–127. https://doi.org/10.1021/acsenvironau.1c00032.
Zhang, Q., Hu, J., Lee, D.-J., Chang, Y., Lee, Y.-J., 2017. Sludge treatment: current research trends. Bioresour. Technol. 243, 1159–1172. https://doi.org/10.1016/j.biortech.2017.07.070.
Zhang, X., Yuan, X., Yang, X., Yang, Z., Han, L., 2026. Two-dimensional correlation infrared spectroscopy reveals the evolution of functional groups governing biochar oxidation resistance. Sci. Rep. 16, 1565. https://doi.org/10.1038/s41598-025-29539-5.
Zhao, L., Cao, X., Mašek, O., Zimmerman, A., 2013. Heterogeneity of biochar properties as a function of feedstock sources and production temperatures. J. Hazard. Mater. 256–257, 1–9. https://doi.org/10.1016/j.jhazmat.2013.04.015.
Zhou, Y., Li, D., Li, Z., Guo, S., Chen, Z., Wu, L., Zhao, Y., 2023. Greenhouse gas emissions from soils amended with cornstalk biochar at different addition ratios. Int. J. Environ. Res. Public Health 20, 927. https://doi.org/10.3390/ijerph20020927.